Extraction of second-order cyclostationary sources by matching instantaneous power spectrum with stochastic model – application to wind turbine gearbox

Ge Xin, Nacer Hamzaoui, Jérôme Antoni

Renewable Energy 147 (2020) 1739–1758

Contents lists available at ScienceDirect

Renewable Energy

journal homepage: www.elsevier.com/locate/renene

Extraction of second-order cyclostationary sources by matching instantaneous power spectrum with stochastic model – application to wind turbine gearbox

Ge Xin [a, b, c], Nacer Hamzaoui [b], Jérôme Antoni [b, *]

[a] School of Traffic and Transportation, Beijing Jiaotong University, Beijing, 100044, PR China
[b] Laboratoire Vibrations Acoustique, Univ Lyon, INSA-Lyon, LVA EA677, F-69621, Villeurbanne, France
[c] Beijing Research Center of Urban Traffic Information Sensing and Service Technologies, Beijing Jiaotong University, Beijing, 100044, PR China

ARTICLE INFO

Article history:
Received 12 April 2019
Received in revised form
29 August 2019
Accepted 16 September 2019
Available online 19 September 2019

Keywords:
Wind turbine gearbox
Machinery fault diagnosis
Semi-blind feature extraction
Cyclic source separation
Cyclostationary signals

ABSTRACT

The diagnosis of gearboxes plays a crucial role in the maintenance of wind turbine. Considering critical elements – i.e. gears and bearings – of gear set, the effective and exact identification of fault sources is appealing yet challenging in complex mechanical systems. Although rotating machine signals are perfectly modelled as cyclostationary (CS) processes, very few researches have so far tried to refine single CS component of interest from a mixture of multi sources; thus the efficacy of classical vibrodiagnostic tool (e.g. envelope analysis) can be greatly enhanced in a wide variety of situations, e.g. poly-cyclostationary cases in wind turbine gearboxes. As such, this paper exploits the statistical behavior of CS signals using a stochastic model based on a periodic variance to extract more specific information from the data themselves. In particular, a statistical indicator is proposed to assess the strength of CS components as well as a full-band time-dependent filter to recover the pure CS signals in the time domain. This proves very useful in many situations where the characteristic components of gears and/or bearings are embedded in heavy background noise that jeopardize their detection in practical applications. The derivation of the proposed scheme is described in detail. Its effectiveness is finally demonstrated with both synthetic and experimental examples.

1. Conventions

Vibration-based source separation is the issue of extracting individual but physically different sources from vibration measurements: periodic, random stationary and random nonstationary [1,2]. The mixtures can be supposed to be additive, multiplicative or convolutive, depending on the physical nature of the application.

The connections between the source *contributions* handled in the paper are schemed in Fig. 1.

For a complex system such as a wind turbine gearbox, it is highly recommended to separate only one signal of interest (SOI) – which implies cyclostationarity – in an iterative way, rather than trying to handle *all* sources at once. The strategy is based on the assumption of stationary speed fluctuations, while recognizing deterministic (purely periodic) and random (quasi-cyclostationary) signals as being first- and second-order cyclostationary ones in presence of additive interactions. It is emphasized that the other sources may be either stationary or cyclostationary as long as their cyclic frequencies are different from that of the source to be extracted.

2. Introduction

Wind energy presents one of the most important resources for human being thanks to its properties of cleanliness and renewability. As widely known, since wind is generated by temperature differences between air masses, wind turbines are typically installed in rough hard-to-reach places where hostile weather and high waves make the maintenance task rather challenging and expensive [3].

The topic on fault diagnosis and condition monitoring of wind turbines has attracted growing interest in the scientific community as mentioned in many review articles [4–8]. Gearboxes and generators are main but fragile parts in drive trains due to the issues of

* Corresponding author.
E-mail addresses: ge.xin@bjtu.edu.cn (G. Xin), jerome.antoni@insa-lyon.fr (J. Antoni).

https://doi.org/10.1016/j.renene.2019.09.087
0960-1481/

Nomenclature

t	time variable (in s)
τ	time-lag (in s)
f	spectral (or carrier) frequency (in Hz)
Δf	frequency resolution in f (in Hz)
f_k	k-th discrete frequency (in Hz)
α	cyclic (or modulation) frequency (in Hz)
$x(t)$	signal of interest
P_x	signal power
$P_x(t)$	mean instantaneous power
$P_x(f)$	power spectral density
$P_x(t;f,\Delta f)$	instantaneous power spectrum
$x_{\Delta f}(t;f)$	filtered signal in the frequency band $[f - \Delta f/2; f + \Delta f/2]$
$WV_x(t;f)$	Wigner-Ville spectrum
AIPS	Averaged Instantaneous Power Spectrum
DFT	Discrete Fourier Transform
STFT	Short-Time Fourier Transform
SES	Squared Envelope Spectrum
$w[n]$	data window (function of time index n)
$X_{STFT}(i,f)$	STFT coefficient at time index i and frequency f
L	signal length
N_w	window length in STFT
R	block shift in STFT
K	total number of blocks used in spectral estimates
F_s	sampling frequency
t_n	n-th discrete time instant (in s)
T	cyclic period of a cyclostationary signal (in s)
α	cyclic (or modulation) frequency (in Hz)
α_{max}	maximum analyzed cyclic frequency (in Hz)
$R_x(t_n,\tau)$	instantaneous autocorrelation function of signal x
$S_x(\alpha,f)$	Spectral Correlation of signal x
$S_x^{SES}(\alpha)$	Squared Envelope Spectrum of signal x

high impact and mechanical strength, and thus foremost causes of wind turbine downtime [9,10]. Furthermore, bearings cause more than 50% of faults on gearboxes, and therefore 50% of all costs associated to these faults [4]. Consequently, the conditioning monitoring of wind turbine bearings has also become a priority to limit premature failures.

Bearings are vulnerable yet essential components of wind turbines as well as in other rotating machines widely serving in heavy industry, such as aerospace, automotive and transmission systems. Typical bearing defects are caused by cracks, breakages, spalls or uneven wear (pitting, scuffing, abrasion, erosion), often located on the matting surface of the inner race, the outer race or the rolling elements. As the rolling element strikes a defect, the ensuing vibration signal typically consists of a series of repetitive transients occurring at a specific rate called “bearing characteristic frequency”. Intuitively, each transient resembles a damped impulse response with specific frequency content corresponding to the excited structural resonances, periodically triggering fault signature because of the inherent operation of a machine.

Therefore, fault detection involves a process of signal demodulation. The prevailing method in the modern literature is surely the squared envelope spectrum (SES). The envelope spectrum is a mean to demodulate a nonstationary signal – of possible random nature, in particular cyclostationary – and identify periodic modulations related with the bearing characteristic frequencies [11]. While, the fact that the SES of the raw signal is rarely a good diagnostic indicator when used without pre-processing, because it is highly sensitive to the presence of background noise and other interfering components [12–14]. Thus, this issue has been addressed and has led to the use of the SES in combination with different pre-processing tools apt to identify the optimal demodulation band, for instance rooted on the spectral kurtosis – computed with the fast kurtogram – as an effective measure of the ‘impulsiveness’ hidden in a signal [15,16]. A recent extension of the kurtogram, with similar goal but refined properties, is the infogram [17–19]. Many wavelet filtering method have been developed by introducing a band pass filter around the resonance frequency of the bearing signature [20–22]. Other approaches – possibly used in conjunction with the latter ones – are based on first denoising the signals by various techniques before computing the SES [23–26]. In summary, the success of the diagnosis of complex systems primarily depends on the validity of source separation (or extraction) process. By this means, the following analysis will be significantly robust in harsh situations without need of pre-processing step.

As a research hotspot, cyclostationary (CS) processes, whose statistics (e.g. the auto-correlation function) varies periodically as a function of time, has been employed in a large amount of fruitful researches for mechanical fault diagnosis [27,28], such as bearings [12,29], gears [30] and so forth [31,32]. Additionally, a great interest has been given to source separation of processes induced by CS properties. Of particular interest is the way of filtering the original signals, that indicates how to decipher the nature of

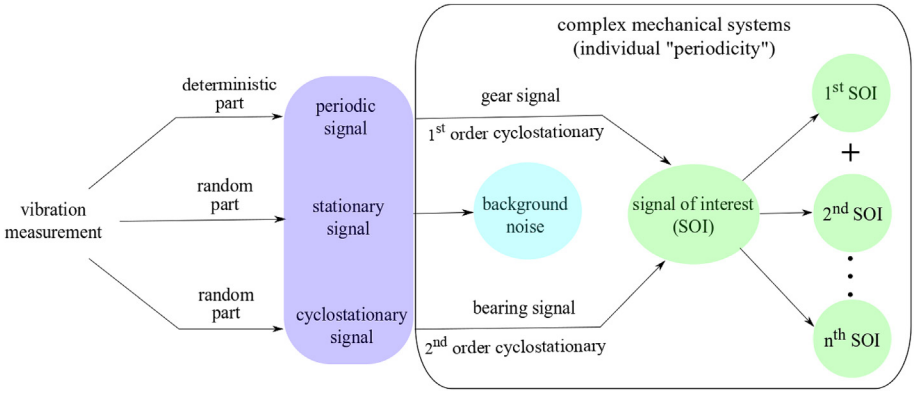

Fig. 1. Structure of vibration signals handled in the paper.

cyclostationarity, such as linear periodically time-varying filters (LPTV) [33], SUBspace BLind EXtraction (SUBLEX) [34], cyclic Wiener filter [35], averaged instantaneous power spectrum (AIPS) [36,37] and time-varying filters [25,38], etc. However, it seems that so far researchers have preferred to employ analytical approaches (aforementioned methods) to separate CS signals (bearing or gear faults), rather than data-driven ones which imply learning the signal structure from the data.

In this paper, a novel stochastic model, whose aim is to extract a CS SOI in the presence of competing sources (background noise and interfering signals) is proposed. It proceeds from only a priori known cyclic frequency of the SOI – which may be estimated beforehand, for instance with the fast spectral correlation [28]. Next, a statistical indicator is proposed to assess the strength of CS components as well as a full-band time-dependent filter to recover the SOI in time domain. Finally, the filtered signal is analyzed by performing the conventional SES, thus showing a significant enhancement as compared to that of the original signal. In addition, it easily allows the use of several cyclic frequencies, which yields a more accurate estimation of the SOI, for instance while handling the case of two sources (bearing and gear signals) in wind turbine gearbox.

The organization of this paper is as follows. In Section 2, a brief review of the wind turbine layout, its mechanical properties and its problem statement is presented. After a reminder about the concept of the AIPS, Section 3 introduces a novel stochastic model for CS signals on the second-order. Next, in Section 4, an iterative method that alternates between the extraction of the SOI and estimation of the parameters is developed in the maximum-a-posterior sense. A discussion on parameter setting and algorithm initialization is presented in Section 5, which is also demonstrated with synthetic signals. Finally, Section 6 illustrates the application of the proposed methodology on actual vibration signals and compares it with the classical methodology based on the (fast kurtogram + filteration + SES) sequence.

3. Problem statement in wind turbines

Fig. 2 displays a typical layout of a wind turbine. Driven by the wind power, the turbine rotor can transmit wind energy into mechanical energy, via the main shaft through the gearbox to the generator. The 3-stage gearbox has the function to optimize the generator speed to be as suitable as possible for the generation of electricity. For instance, it is generally designed as planetary and sun gear (with the standstill ring gear) with parallel gear structure to achieve higher transmission ratio and output power within compact space. The parallel gear has three shafts: the slow speed shaft connected to the sun shaft, the intermediate speed shaft and the high speed shaft used in combination to drive the generator.

As a typical case of complex systems, a wind turbine contains several components rotating at different speeds. For instance the wind turbine of Fig. 2 contains 3 main sources – i.e. 17 rolling element bearings, 9 gears and 8 shafts – likely to release energy. It should be re-emphasized that the rolling element bearings are numerous, crucial but fragile components of gearboxes. Therefore and due to its practical importance, the bearing source is a priority to analyze among the others. As pointed out previously, bearing damage triggers repetitive impacts of the moving components on the defect, i.e. the inner race, the outer race or the rolling elements. As a matter of fact, such diagnostic information is often masked by numerous extraneous sources of vibration, simply referred to hereafter as “background noise”. For instance, they are mostly gear mesh components modulated by the shaft speed, which usually dominate the lower frequency range (up to around 5 kHz). It often happens that the major resonance frequencies of bearing signals is relatively higher than that of gear signals, whereas these different frequency ranges add more challenges to wind turbine monitoring, mainly due to cross frequencies and low frequency bursts.

4. Proposal of a periodic-variance based model

4.1. The concept of instantaneous power spectrum

Let $y(t_n)$ denote the measured signal in the time domain where $t_n = n/F_s$ refers to time instants acquired with sampling frequency F_s. Whenever convenient, the stream of samples $y(t_n)$, $n = 0,\ldots,L-1$, will be simply denoted by $y[n]$. By convention, it consists of the SOI $x[n]$ and the residual part $r[n]$ denoted “background noise” in presence of additive interactions. The measured signal is thus expressed by the linear combination

$$y[n] = x[n] + r[n]. \tag{1}$$

Although $r[n]$ probably comprises multiple components (or even the other SOI of minor importance), it intervenes in model (1) as a wide-sense “background noise”. It is noteworthy that their exact separations are not necessary at this stage, yet they may be either

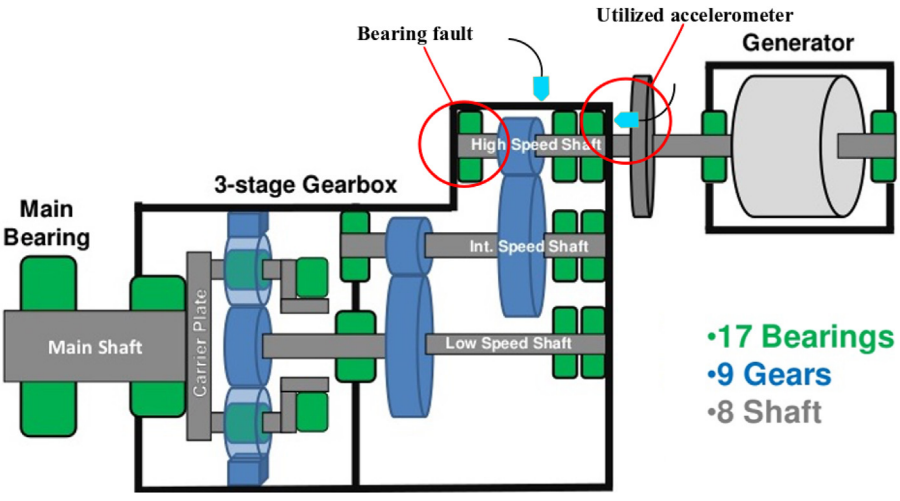

Fig. 2. Layout of a typical wind turbine: a complex structure with several components.

periodic or cyclostationary as long as their basic cycles are different from that of the source to be extracted. In contrast, since $x[n]$ represents the fault signal in its early stage, it is well modelled by a series of impacts that repetitively excite resonances of the bearing and of its receiving structure, thus leading to successive damped impulse responses. Having a localized signature both in time and in frequency, such transients are well captured in a time-frequency decomposition. Although several time-frequency decompositions are possible, the proposed approach only requires an invertible one. The STFT meets this property while being associated with efficient algorithmic implementations. In addition, due to the Central Limit Theorem applied to the DFT (discrete Fourier Transform), the coefficients of the STFT quickly tend in distribution to a complex-valued Gaussian [39], an assumption that will substantially simplify the probabilistic model introduced hereafter. It is noteworthy that the aim is to decompose the signal without loss of information in the time-frequency domain in which it will be processed; therefore, considerations such as the uncertainty principle will not matter because they are relevant to time-frequency representation (i.e. visual analysis), which is not of concern here.

The STFT of signal $x[n]$ over a time interval of duration N_w/F_s is defined as

$$X(i,f_k)=\sum_{m=0}^{N_w-1} x[iR+m]w[m]e^{-j2\pi f_k\frac{iR+m}{F_s}} \tag{2}$$

where $w[m]$ denotes a positive and smooth N_w-long data-window which truncates a segment of the L-long signal $x[n]$ at time datum i ($i=1,\ldots,N$, $N=\text{floor}\,[(L-N_w)/R+1]$) with window shift R ($1<R<N_w$) and where $f_k=k\Delta f$ denotes the discrete frequencies with frequency resolution

$$\Delta f=\frac{F_s}{N_w} \tag{3}$$

and bin indices $k=0,\ldots,N_f$ ($N_f=N_w/2-1$ if N_w is even and $N_f=(N_w-1)/2$ if it is odd).

The interpretation of $X(i,f_k)$ is the "complex envelope" of signal $x[n]$ in a narrow frequency band of bandwidth Δf centered on f_k and sampled at time instants iR/F_s. Its squared magnitude, $|X(i,f_k)|^2$, thus reflects the energy flow in the frequency band [27]. Moreover, the collection of squared coefficients $|X(i,f_k)|^2$'s for all time indices iR and frequencies f_k defines the spectrogram, which is referred to as the instantaneous power spectrum (IPS). For a CS source, the IPS evidences cyclic behavior *in* and *across* its frequency bins and it appears to be very useful for describing the energy distribution about the signal as a function of time and frequency. From now on, signal $x[n]$ is assumed to be cyclostationary on the second-order. This means that its Wigner-Ville *spectrum*,

$$\mathscr{W}\mathscr{V}_{XX}\left[n,f_k\right)=\mathbb{E}\Big\{\underset{\tau\to f_k}{\mathscr{F}}\Big\{x\Big[n+\tau/2\Big]x\Big[n-\tau/2\Big]^*\Big\}\Big\}, \tag{4}$$

(where n and τ stand for the time instant and the time-lag, $\mathbb{E}$ for the ensemble average operator, $\mathscr{F}$ for "Fourier transform" and $*$ for the complex conjugate) is a poly-periodic function of time n; therefore it can also be expressed by a Fourier series

$$\mathscr{W}\mathscr{V}_{2X}\left[n,f_k\right)=\sum_{\alpha_j\in\mathscr{A}}\mathscr{S}_{2X}\left(f_k;\alpha_j\right)e^{j2\pi\alpha_j n/F_s} \tag{5}$$

over the spectrum $\mathscr{A}=\{\alpha_j\}$ of cyclic frequencies α_j associated with the non-zero Fourier coefficients, $\mathscr{S}_{2X}(f_k;\alpha_j)$, which denotes the cyclic power spectrum (units = power/Hz) [32].

Although the Wigner-Ville distribution (WVD) has been extensively used for identification of rotating machinery spectral components, its usage is still hampered by some problems (e.g., interferences, locally negative values). For instance, because of its uneven performance for different classes of signals, it is not suitable for analyzing wind turbine gearboxes, especially when there is a relatively large dispersion of the energy level. Thus, an alternative distribution is proposed by defining the averaged IPS [36], evolved from the synchronous averaging technique. It has proven that the IPS is amenable to recover CS components masked by other components originated from different sources. It therefore applies to either multi-fault cases or in the presence of high noise disturbances [37]. However, due to the properties of the synchronous averaging operation, it may undergo the influence of artifacts in the presence of random slip. In real life applications, identification of signals can benefit from the stochastic model by adapting its content to fit the data themselves. However it is sometimes impossible to identify them all, and one thus prefers one which already incorporates some prior knowledge about the data.

To this end, a novel stochastic model is proposed to automatically recognize the time-dependent signature of CS components via a pre-selected cycle T, thus resulting in a semi-blind feature extraction.[1] Therefore, an accurate energy distribution over time index n is tailored to the data which leads to high adaptability and flexibility. The goal of designing this model is to approach the behavior of experimental data as close as possible.

4.2. The stochastic model for periodic energy flow

The STFT coefficients $X(i,f_k)$ is defined as a random function of time datum i with frequency index f_k, which follows a time-dependent complex normal distribution,

$$X(i,\,f_k)\sim\mathscr{CN}\Big(0,\,\sigma_x^2(i);\,f_k\Big) \tag{6}$$

where $\mathscr{CN}(\mu,\,\sigma^2(i);\,f_k)$ denotes the circular-symmetric complex normal distribution with mean μ and instantaneous variance $\sigma^2(i)$ applied to frequency f_k. Without loss of generality, it is assumed that $\mu=0$ (as obtained after first centering the signal). It is hereby reminded that in this paper the proposed model consistently regards the frequency f_k as a parameter rather than a variable.[2]

In the case of a second-order CS signal, the distribution (6) exhibits some hidden periodicities in the statistical sense. Intuitively, the cyclic variation of $\sigma_x^2(i)$ evidences the presence of a repetitive behavior in the signal, for instance due to the occurrence of a fault in the form of a series of impulses or in the form of periodic modulations, but not only.

In observations from rotating machinery, the cyclic frequency results from the machine kinematics which is usually known or alternatively can be obtained, for instance by means of the spectral correlation or the squared envelope spectrum. This guarantees a perfect extraction of the SOI in the noiseless case.

For given period T of the component of interest, the time-dependent variance of $Y(i,\,f_k)$ can be described as follows:

[1] Although the method requires the knowledge of the cyclic frequency of the SOI to be extracted, it is worth insisting that it is semi-blind in the sense that the latter can be estimated from the data and that nothing else is assumed (about the number of interferences, their statistics and the noise properties). However, the ensuing procedure will entirely benefit from the accuracy of feature extraction while making the computational complexity acceptable.

[2] This means that the frequency f_k is separable and distinctive from other frequencies. For notational simplicity, it will be dropped off in cases wherein it will not cause any confusion.

$$\sigma_y^2(i;\, f_k) = \sigma_x^2(i;\, f_k) + \sigma_r^2(f_k), \tag{7}$$

where $\sigma_x^2(i;\, f_k) = \sigma_x^2(i + j \times T;\, f_k)$ (T is the periodic time of impacts and j is an integer) and $\sigma_r^2(f_k)$ denotes the variance of additive noise $R(f_k)$ which is assumed time-invariant for simplicity. In words, such processing reflects the hidden repetitiveness of the energy flow in the frequency band f_k, namely periodic-variance based model, which specifying cyclostatioanry signals in the field of machine condition monitoring and fault diagnostics.

5. Extraction of cyclic components of interest

Let us start with the joint posterior probability distribution of the SOI and the model parameters given the observations,

$$p(X(i,\, f_k),\, \boldsymbol{\theta} | Y(i,\, f_k)), \tag{8}$$

where $\boldsymbol{\theta} = \{\sigma_x^2(i),\, \sigma_r^2,\, \alpha_x,\, \beta_x,\, \alpha_r,\, \beta_r\}$ denotes the set of all the unknown parameters.

Under these circumstances, the desired signal $X(i,\, f_k)$ and the parameters $\boldsymbol{\theta}$ may be estimated from the expectation-maximization (**EM**) algorithm

$$\begin{cases} p(X(i,\, f_k) | Y(i,\, f_k),\, \boldsymbol{\theta});\ \textit{a priori known}\ \boldsymbol{\theta} \\ p(\boldsymbol{\theta} | Y(i,\, f_k),\, X(i,\, f_k));\ \textit{a priori known}\ X(i,\, f_k) \end{cases}. \tag{9}$$

The **EM** algorithm makes use of the following quantities.

5.1. Expectation step:extraction of the CS signal

First, the posterior probability distribution of the SOI given the observations and the current parameters $\widehat{\boldsymbol{\theta}}$ is expressed as

$$p(X(i,\, f_k) | Y(i,\, f_k),\, \widehat{\boldsymbol{\theta}}) \propto p(Y(i,\, f_k) | X(i,\, f_k),\, \widehat{\boldsymbol{\theta}}) p(X(i,\, f_k) | \widehat{\boldsymbol{\theta}}). \tag{10}$$

Therefore, combining the above definition (6), it holds that

$$p(X(i,f_k) | Y(i,f_k),\, \widehat{\boldsymbol{\theta}}) = \frac{exp\left\{ \frac{-|Y(i,f_k) - X(i,f_k)|^2}{\widehat{\sigma}_r^2(f_k)} \right\} exp\left\{ \frac{-|X(i,f_k)|^2}{\widehat{\sigma}_x^2(i;\, f_k)} \right\}}{\pi^2 \widehat{\sigma}_r^2(f_k) \widehat{\sigma}_x^2(i;\, f_k)}. \tag{11}$$

After some manipulations, Eq. (11) can be expressed as

$$\begin{aligned} p(X(i,f_k) | Y(i,f_k),\, \widehat{\boldsymbol{\theta}}) &= \frac{exp\left\{ \frac{-|X(i,f_k) - \mu_x(i;\, f_k)|^2}{\sigma_x^2(i;\, f_k)} \right\}}{\pi \sigma_x^2(i;\, f_k)} \\ &= \mathscr{CN}(X(i,f_k);\, \mu_x(i;\, f_k),\, \sigma_x(i;\, f_k)) \end{aligned} \tag{12}$$

with

$$\begin{cases} \sigma_x^2(i;\, f_k) = \left(\dfrac{1}{\widehat{\sigma}_r^2(f_k)} + \dfrac{1}{\widehat{\sigma}_x^2(i;\, f_k)} \right)^{-1} \\ \mu_x(i;\, f_k) = \dfrac{\sigma_x^2(i;\, f_k)}{\widehat{\sigma}_r^2(f_k)} Y(i,f_k) \end{cases}. \tag{13}$$

Therefore the conditional expectation of the signal of interest $X(i,f_k)$ reads

$$\mathbb{E}\{X(i,f_k) | Y(i,f_k),\, \widehat{\boldsymbol{\theta}}\} = \mu_x(i;\, f_k) = \frac{1}{1 + H(i;\, f_k)} Y(i,f_k) \tag{14}$$

where

$$H(i;\, f_k) = \frac{\widehat{\sigma}_r^2(f_k)}{\widehat{\sigma}_x^2(i;\, f_k)} \tag{15}$$

denotes the time-dependent variance ratio between the noise and the CS signal at f_k.

Finally, the time signal $\widehat{x}[n]$ is obtained from Eq. (14) by using the inverse STFT.

Two remarks are noteworthy. First, it is seen that Eq. (14) corresponds to a periodic time-varying filter from which superior performance is expected than from a conventional time-invariant filter. Second, the standard Wiener filter appears as a particular case under the assumption of stationarity, that is

$$\mathbb{E}\{X(i,f_k) | Y(i,f_k)\} = \frac{1}{1 + \frac{\widehat{\sigma}_r^2(f_k)}{\widehat{\sigma}_x^2(f_k)}} Y(i,f_k), \tag{16}$$

where the time index i of the time-dependent variance $\widehat{\sigma}_x^2(i;\, f_k)$ stays constant for all time instants. In other words, Eq. (16) then corresponds to the case where $\sigma_y^2 = \sigma_x^2 + \sigma_r^2$ instead of Eq. (7).

5.2. Maximization step:estimation of unknown parameters

Next, let consider the posterior probability distribution of the unknown parameters given the observations and the current $\widehat{X}(i,\, f_k)$, expressed as

$$p(\boldsymbol{\theta} | Y(i,\, f_k),\, \widehat{X}(i,\, f_k)) \propto p(Y(i,\, f_k) | \widehat{X}(i,\, f_k),\, \boldsymbol{\theta}) p(\boldsymbol{\theta} | \widehat{X}(i,\, f_k)). \tag{17}$$

By definition, the unknown shape and scale parameters $\{\alpha_x,\, \beta_x,\, \alpha_r,\, \beta_r\}$ will be estimated and kept constant in the procedure of data-driven initialization. As a result, $\boldsymbol{\theta}$ consists of the unknown parameters $\{\sigma_x^2(i),\, \sigma_r^2\}$ hereafter.

The time-dependent variance is therefore defined as a hidden variable, which is referred to as the inverse gamma distribution

$$\sigma^2(i) \sim Inv - Gamma(\alpha,\, \beta) \tag{18}$$

with shape parameter α and scale parameter β. For example, $\sigma_x^2(i) \sim Inv - Gamma(\alpha_x,\, \beta_x)$ and $\sigma_r^2(i) \sim Inv - Gamma(\alpha_r,\, \beta_r)$ stand for the time-dependent variance of $x[n]$ and $r[n]$, respectively.

Along these lines, in the case of proposed stochastic model, $\sigma_x^2(i)$ and σ_r^2 are further assigned informative priors[3] in the form of analytically tractable conjugate distributions[4]

$$\begin{aligned} p\left(\sigma_x^2(i;\, f_k) \middle| Y(i,\, f_k),\, \widehat{X}(i,\, f_k) \right) &\sim Inv \\ &- Gamma\left(\alpha_x + \frac{N}{2},\, \beta_x + \frac{N}{2} \mathscr{P}\left\{ |X(i,\, f_k)|^2 \right\} \right) \end{aligned} \tag{19}$$

where $\mathscr{P}\{\bullet\}$ is the poly-periodic extraction operator [27], defined as follows

[3] This expresses specific, definite information about a variable that is determined largely by pre-existing evidence rather than any original assumption; the terms "prior" and "posterior" are generally relative to a specific datum or observation. A reasonable approach is to make the prior parametrization with expected value and variance value as schemed in Eq. (24).

[4] It is proved that the inverse gamma distribution is a conjugate prior of the complex normal distribution where $p(\sigma^2 | y[n],\, \mu) \sim Inv - Gamma\left(\alpha + \frac{n}{2},\, \beta + \sum_{i=1}^{n} \frac{|y_i - \mu|^2}{2} \right)$, more details are shown in Ref. [40].

$$\mathscr{P}\{\bullet\} = \sum_{\alpha \in \mathscr{A}} \mathscr{P}_\alpha\{\bullet\} \tag{20}$$

where the set $\mathscr{A}$ contains all cyclic frequencies α associated with non-zero periodic components. In particular, the $\mathscr{P}_\alpha$-operator first computes the Fourier coefficient at frequency α and then assigns it to that periodic component $\exp(j2\pi\alpha t)$ in order to reconstruct a pure sinusoidal signal, defined as follows

$$\mathscr{P}_\alpha\{\bullet\} = \left(\lim_{T\to\infty} \frac{1}{T}\int_T (\bullet) e^{-j2\pi\alpha t} dt\right) \cdot e^{j2\pi\alpha t}. \tag{21}$$

In this case, let us first calculate the expectation of cyclic modulation spectrum (CMS)

$$\widehat{P}_{2X}(f_k;\alpha_j) = \frac{1}{N}\sum_{i=1}^{N} |\widehat{X}(i,f_k)|^2 e^{-j2\pi\alpha_j iR/F_s} \tag{22}$$

with a collection of parallel cyclic spectra $\mathscr{A} = \{\alpha_j\}$ at the discrete cyclic frequencies $\alpha_j = j/T$. It results from the property that, for a CS stochastic process, the alignment of non-zero Fourier coefficients only appear on a countable set of frequencies, i.e. α_j.

According to Eq. (20)-(21), the instantaneous power spectrum $P_{2X}(i,f_k)$ is then computed as follows

$$\mathscr{P}\left\{|X(i,f_k)|^2\right\} = \sum_{\alpha_j \in \mathscr{A}} \widehat{P}_{2X}(f_k;\alpha_j) e^{j2\pi\alpha_j iR/F_s}. \tag{23}$$

Now let us remind the property of $Inv-Gamma(\alpha,\ \beta)$ parametrization with

$$\begin{cases} \mathbb{E}\{\sigma^2\} = \dfrac{\beta}{\alpha-1} & \text{for } \alpha > 1 \\ Var\{\sigma^2\} = \dfrac{\beta^2}{(\alpha-1)^2(\alpha-2)} & \text{for } \alpha > 2 \end{cases}. \tag{24}$$

Taking the expected value of $\sigma_x^2(i;\ f_k)$, one arrives at

$$\mathbb{E}\left\{\sigma_x^2(i;\ f_k)\right\} = \frac{\beta_x + \frac{N}{2}\mathscr{P}\left\{|X(i,\ f_k)|^2\right\}}{\alpha_x + \frac{N}{2} - 1}. \tag{25}$$

The above equation is a fundamental step towards the dynamic behavior of experimental data in a statistical sense. It not only returns the repetitively distributed variance which indicates the CS source, but provides also quantification of their significance which highlights the results of this paper.

In the stochastic framework, let $CS(f_k)$ denote the statistical index at frequency f_k, obtained by taking the standard deviation of $\sigma_x^2(i;\ f_k)$ over the time instants i, expressed as follows

$$CS(f_k) = \sqrt{\frac{1}{N-1}\sum_{i=1}^{N}\left(\sigma_x^2(i;\ f_k) - \overline{\sigma_x^2}(f_k)\right)^2} \tag{26}$$

where $\overline{\sigma_x^2}(f_k)$ is the mean value of the time-dependent variance. It is noteworthy that $CS(f_k)$ is a cyclostationary index on the fourth-order that is apt to measure the "depth" of a modulation with frequency $\alpha = 1/T$ Hz at carrier frequency f_k.

Likewise, the expectation of the time-invariant variance $\sigma_r^2(f_k)$ is expressed as

$$\mathbb{E}\left\{\sigma_r^2(f_k)\right\} = \frac{\beta_r + \sum_{i=1}^{N}\frac{|Y(i,f_k) - \widehat{X}(i,f_k)|^2}{2}}{\alpha_r + \frac{N}{2} - 1} \tag{27}$$

which appears as a particular case under the stationary assumption of the noise.

By now, the ***M**aximization* step is completely introduced and it will alternate with the ***E**xpectation* step in the iterative process, thus driving the convergence of the proposed **EM** algorithm.[5] The performance of the proposed extraction scheme will be respectively demonstrated on synthetic and experimental signals in subsection 5.3 and 6.

6. Parameter setting, algorithm initialization and demonstration

6.1. Parameter setting

The proposed methodology is based on the decomposition of the signal by means of the STFT. Therefore, the first required parameters to tune are the window length N_w and the window shift R (see Eq. (2)).

6.1.1. Window length N_w

The value of N_w directly controls the frequency resolution (see Eq. (3)), which characterizes the carrier frequency. It is recommended that it covers at least the duration T_I of a transient, which implies the condition

$$\Delta f < 1/T_I. \tag{28}$$

As the STFT is subjected to the uncertainty principle, $\Delta t \Delta f \geq 1$, the highest cyclic frequency of $\sigma_x^2(i)$, $\alpha_{max} = 1/\Delta t$, is bounded upward by Δf [27]. Therefore the available range of hidden variables is limited by

$$\alpha_{max} \leq \Delta f. \tag{29}$$

Accordingly, N_w should be taken short to allow a relatively high varying rate in Eq. (29), but long enough to satisfy Eq. (28), i.e. $F_s \cdot T_I < N_w \leq F_s \cdot \Delta t$ as illustrated in Fig. 3.

Other reasons for taking N_w small is to reduce the computation time required by the STFT and also to ensure sufficient segments for accurate parameter estimation.

It is noticed here that the rule for setting N_w also works in the special case where the interval Δt between adjacent transients is close to the impulse duration T_I. In other words, it is robust enough to balance the trade-off between a fine resolution and a high cyclic frequency of hidden variables. As long as the selected N_w respects the conditions of Eqs. (28) and (29), it is possible to run the proposed algorithm with a few tentative windows, ranging logarithmically (e.g. the powers of two), and eventually to obtain the best result of all. These facts will be further verified by real-world signals in Section 6.

6.1.2. Window shift R

There are two considerations for the window shift R:

- first, for the STFT to be invertible, it is recommended to take at least 75% overlap with a Hanning window,

[5] According to the Zangwill's global convergence theorem [41], the proof of convergence of the proposed **EM** algorithm (for computing maximum a posteriori estimate) to the stationary points of the posterior density function is studied in great detail in Ref. [42].

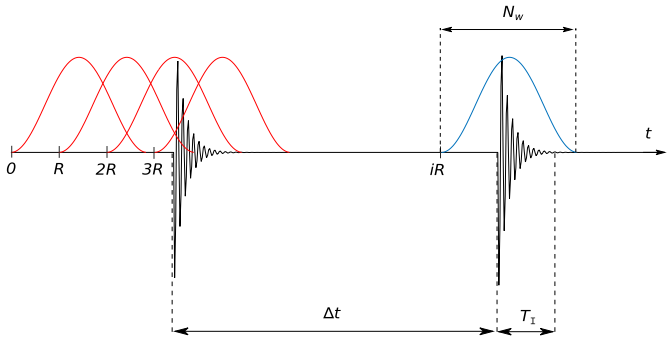

Fig. 3. Illustration of how to select the window length N_w and shift R with respect to transient durations T_I and cycle Δt.

- second, if invertibility is not required, R should be taken sufficiently small to keep enough diagnostic information while not increasing too much computational cost and the dependence between adjacent segments; a typical choice is within 50% and 75% overlap with a Hanning window.

Therefore, the window shift can be easily set by default.

6.2. Initializing parameters of the EM algorithm

The **EM** algorithm generally requires a good initialization step in consideration of two reasons. The first ones is to avoid being trapped in possible local maxima of the posterior and the second one is to achieve a fast convergence speed. A simple self-running solution is given hereafter to obtain initial values along the frequency indices f_k step-by-step.

The initialization of spectral components runs in an iterative way, i.e. $f_{k-1} \rightarrow f_k$ (bin index $k = 2, \ldots, N_f$), so as to start with the initial variance of noise

$$\mathbb{E}\left\{\sigma_r^2(f_k)\right\}^{[0]} = \frac{1}{N}\sum_{i=1}^{N}\left|Y(i, f_{k-1}) - \widehat{X}(i, f_{k-1})\right|^2. \tag{30}$$

This operation is based on the assumption that the measurement $Y(i, f_k)$ embodies the CS signal $X(i, f_k)$ in the presence of stationary noise $N(f_k)$. Whereafter, the initial time-dependent variance of the CS signal is approximated by the subtraction

$$\mathbb{E}\left\{\sigma_x^2(i; f_k)\right\}^{[0]} = \mathscr{P}\left\{|Y(i, f_k)|^2\right\} - \mathbb{E}\left\{\sigma_r^2(f_k)\right\}^{[0]}. \tag{31}$$

Next, according to Eq. (24), one can estimate the shape and scale parameters of noise from

$$\begin{cases} \widehat{\alpha}_r(f_k) = \dfrac{\left(\mathbb{E}\left\{\sigma_r^2(f_k)\right\}^{[0]}\right)^2}{Var\left\{\sigma_r^2(f_k)\right\}^{[0]}} + 2 \\ \widehat{\beta}_r(f_k) = (\widehat{\alpha}_r(f_k) - 1) \times \mathbb{E}\left\{\sigma_r^2(f_k)\right\}^{[0]} \end{cases} \tag{32}$$

where the initial variance of $\sigma_r^2(f_k)$ can be taken as large as possible to achieve a wide dispersion e.g. $Var\{\sigma_r^2(f_k)\}^{[0]} = 10 \times \mathbb{E}\{\sigma_r^2(f_k)\}^{[0]}$. Similarly, for that of the CS signal,

$$\begin{cases} \widehat{\alpha}_x(f_k) = \dfrac{\left(\mathbb{E}\left\{\sigma_x^2(f_k)\right\}^{[0]}\right)^2}{Var\left\{\sigma_x^2(f_k)\right\}^{[0]}} + 2 \\ \widehat{\beta}_x(f_k) = (\widehat{\alpha}_x(f_k) - 1) \times \mathbb{E}\left\{\sigma_x^2(f_k)\right\}^{[0]} \end{cases} \tag{33}$$

where the initial variance of $\sigma_x^2(f_k)$ can be taken as $Var\{\sigma_x^2(f_k)\}^{[0]} = 10 \times \mathbb{E}\{\sigma_x^2(f_k)\}^{[0]}$ and the initial expectation of $\sigma_x^2(f_k)$ as $\mathbb{E}\{\sigma_x^2(f_k)\}^{[0]} = \frac{1}{N}\sum_{i=1}^{N}\mathbb{E}\{\sigma_x^2(i; f_k)\}^{[0]}$.

Of particular importance is the initialization at frequency f_1, which is a special case of the above steps. Specifically, taking the mean value of the squared magnitude of measurement $Y(i, f_1)$, one can obtain the initial variance of noise as

$$\mathbb{E}\left\{\sigma_r^2(f_1)\right\}^{[0]} = \frac{1}{N}\sum_{i=1}^{N}|Y(i, f_1)|^2. \tag{34}$$

Then the initial time-dependent variance of the CS signal reads

$$\mathbb{E}\left\{\sigma_x^2(i; f_1)\right\}^{[0]} = \left(\mathscr{P}\left\{|Y(i, f_1)|^2\right\} - \mathbb{E}\left\{\sigma_r^2(f_1)\right\}^{[0]}\right)_+ \tag{35}$$

where operator $(\ldots)_+$ keeps only the positive value of a quantity.

Next, the shape and scale parameters of noise can be initialized by following Eq. (32); to the contrary, the parameters of the CS signal are taken as $\widehat{\alpha}_x(f_1) = 0$ and $\widehat{\beta}_x(f_1) = 0$ to avoid the risk of overfitting.

It has been observed in numerous experiments that the proposed initializations are often quite close to the maximum a posteriori estimates (global maximum) while allowing at the same time a fast convergence speed of the **EM** algorithm. This will be demonstrated in the next subsection.

6.3. Cases 1 & 2: demonstration of parameter selection

To demonstrate the performance of the proposed algorithm, a synthetic random signal is generated with a resonance frequency $f_0 = 0.1$ Hz which is further modulated by a relatively high fault frequency $\alpha_0 = 5 \times 10^{-3}$ Hz ($T = 1/\alpha_0 = 200$ s, the sampling frequency is normalized to $F_s = 1$ Hz). More precisely, the produced signal is described as:

$$y(t) = \sum_{j=-\infty}^{+\infty} h(t - jT) + n(t) \tag{36}$$

$$H(z) = \frac{b_1}{a_1 + a_2 \cdot z^{-1} + a_3 \cdot z^{-2}} \tag{37}$$

where $n(t)$ denotes white noise that achieves a noise-to-signal-ratio of 6 dB and the signal length is $L = 10^4$ samples. A second-order system is defined by Eq. (37), whose numerator and denominator coefficients are $\boldsymbol{b} = [1]$ and $\boldsymbol{a} = [1, -2cos(2\pi f_0)r, r^2]$ with $r = 0.95$, respectively. Fig. 4 shows the spectrogram (magnitude of the STFT) of the raw signal, with its periodic energy flow, with period T (dashed line in red). The time record is displayed in Fig. 5 (a).

Following Eqs. (30)-(35), one can initialize the parameters $\widehat{\sigma}_x^2(i; f_k)^{[0]}$, $\widehat{\sigma}_x^2(f_k)^{[0]}$ and $\widehat{\sigma}_r^2(f_k)^{[0]}$ as shown in Fig. 6 (a) and Fig. 7 (a).

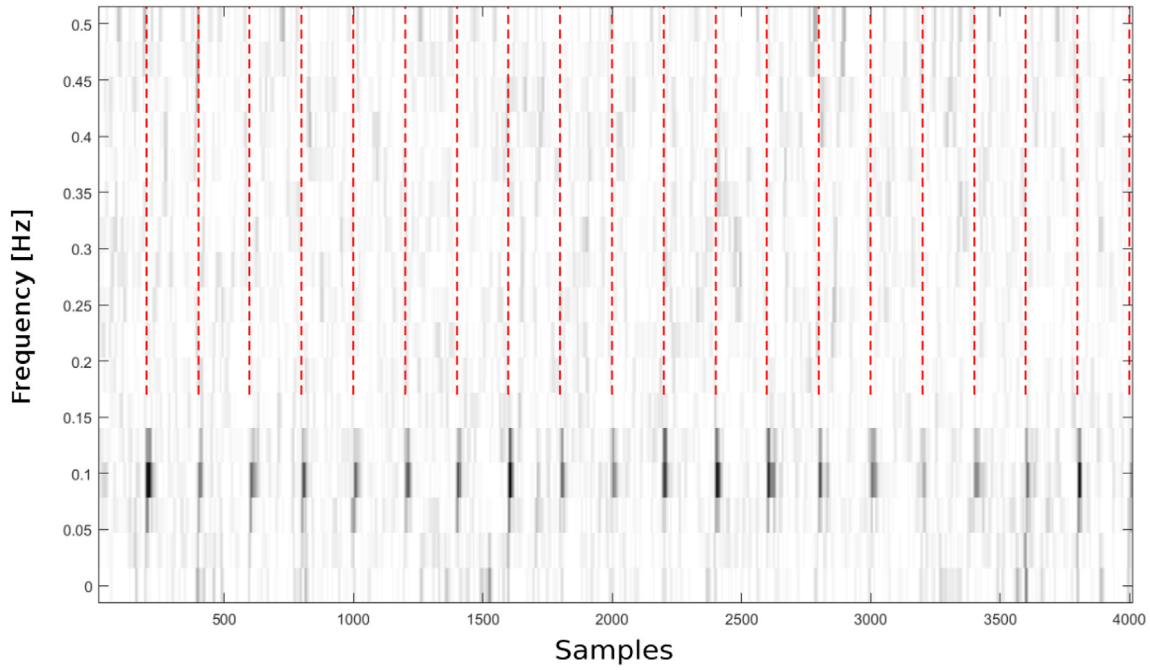

Fig. 4. Spectrogram of the signal simulated in Case 1 with resonance frequency $f_0 = 0.1$ Hz, $r = 0.95$ and fault frequency $\alpha_0 = 5 \times 10^{-3}$ Hz ($T = 1/\alpha_0 = 200$ s, $N_w = 2^5$ and $R = 4$).

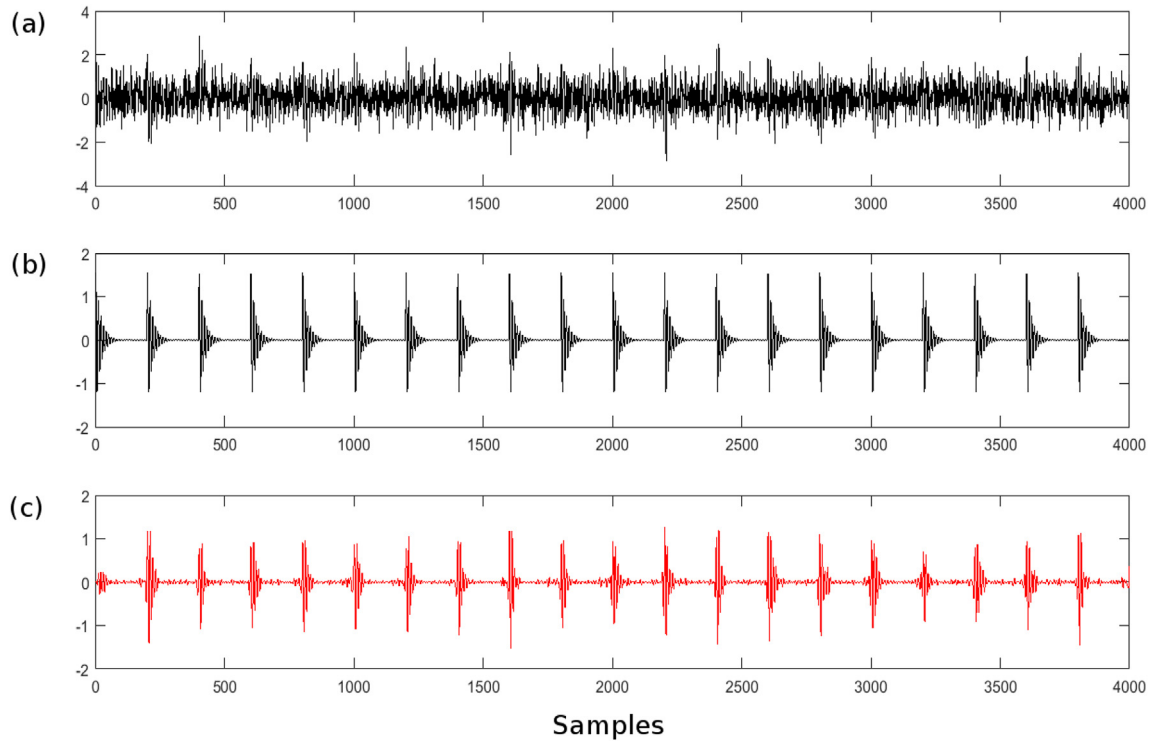

Fig. 5. (a) Synthetic signal of Case 1 with additive white noise (noise-to-signal-ratio = 6 dB. (b) Synthetic transient signal. (c) Filtered time signal $x[n]$.

It is seen that the proposed initialization is simple and effective, even though the estimated spectrum of the signal of interest still contains a significant contribution from noise especially beyond 0.18 Hz. After convergence of the **EM** algorithm, the estimated signal and noise spectra, $\widehat{\sigma}_x(f_k)^{[k+1]}$ and $\widehat{\sigma}_r(f_k)^{[k+1]}$, are close to the theoretical quantities as can be seen in Fig. 7 (b). In particular, the very good estimation of the variance $\widehat{\sigma}_x(i; f_k)^{[k+1]}$ is displayed in Fig. 6 (b) and further reflected by the cyclostationary index $CS(f_k)$ in Fig. 8.

Finally, the filtered time signal $\widehat{x}[n]$ is displayed in Fig. 5 (c), as obtained by using the inverse STFT of the estimated CS signal, $\widehat{X}(i, f_k)$. The corresponding time-varying filter is shown in Fig. 6 (c) and (d), respectively.

To highlight the performance of the proposed extraction

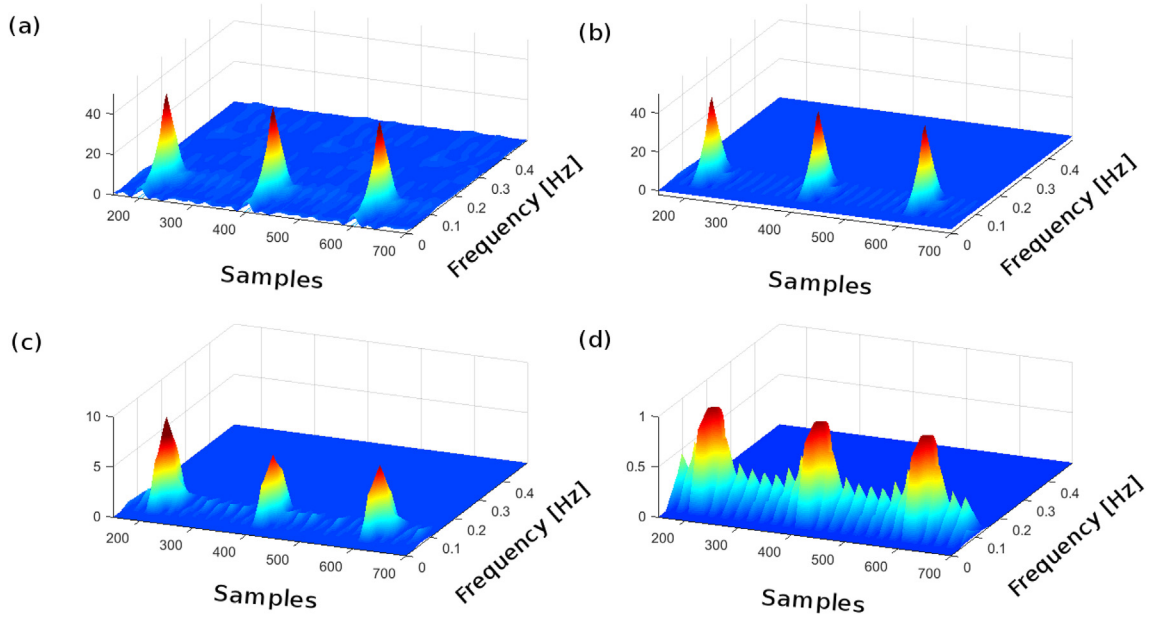

Fig. 6. (a) Initialized time-dependent variance of the CS signal, $\widehat{\sigma}_x^2(i;f_k)^{[0]}$, and (b) the estimated $\widehat{\sigma}_x^2(i;f_k)^{[k+1]}$ from the **EM** algorithm. (c) Spectrogram of the estimated CS signal, $\widehat{X}(i,f_k)$, with (d) its periodic time-varying filter $1/(1+H(i;f_k))$ as defined in Eqs. (14)-(15).

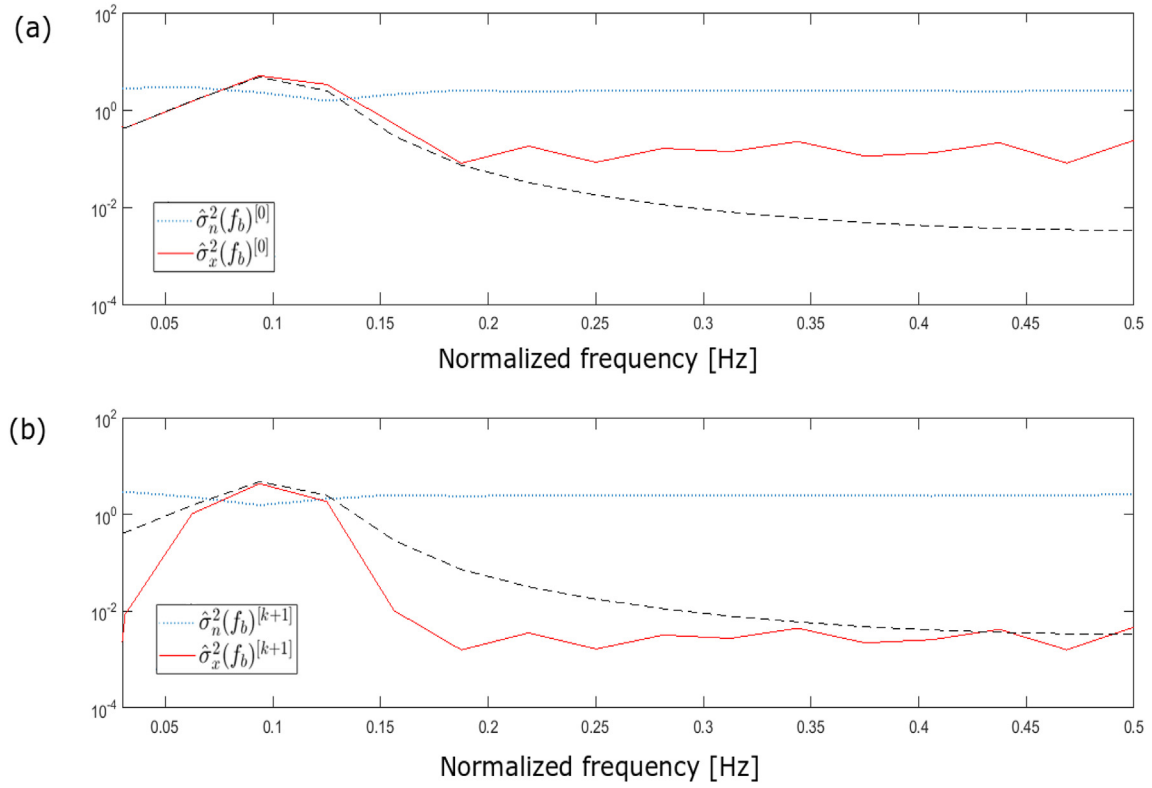

Fig. 7. (a) Initialized spectra (variance of noise and CS signals $\widehat{\sigma}_r^2(f_k)^{[0]}$ and $\widehat{\sigma}_x^2(f_k)^{[0]}$, in blue dotted line and red line, respectively) and (b) estimated spectra from the **EM** algorithm, $(\widehat{\sigma}_r^2(f_k)^{[k+1]}$ and $\widehat{\sigma}_x^2(f_k)^{[k+1]}$, in blue dotted line and red line, respectively) together with the theoretical squared magnitude frequency response $|H(z)|^2$ (black dashed line). (For interpretation of the references to colour in this figure legend, the reader is referred to the Web version of this article.)

scheme, Fig. 9 (a) shows a better view of the recovered time signal $\widehat{x}[n]$ superposed with synthetic transient signal. It is noticed that the extracted CS signal is composed of all the spectra, yet only dominated by the major resonance frequencies with the higher weight. This property can also be verified by the initialized parameter $\widehat{\sigma}_x^2(i;f_k)^{[0]}$, even though it still embodies some marginal spectral contents in Fig. 9 (b). After the iterative steps of the **EM** algorithm, there remain only the components from the CS signal as can be seen in Fig. 9 (c) associated with Fig. 8.

It is well known that in rotating machines various rotations of

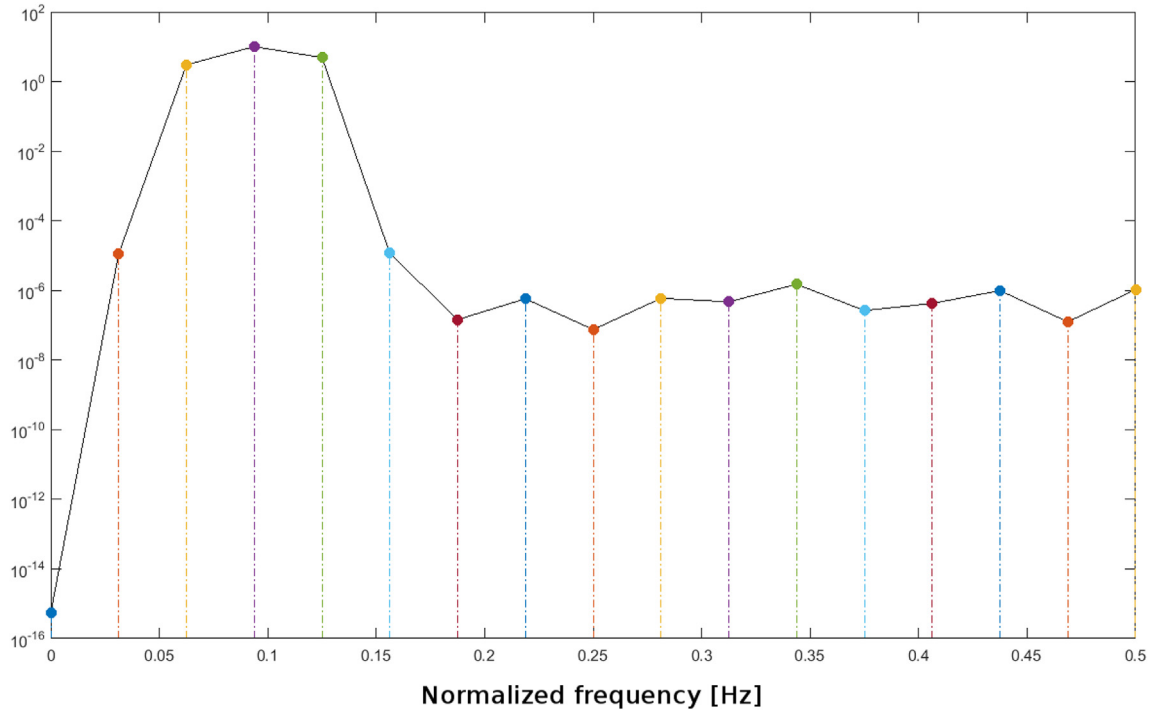

Fig. 8. Cyclostationary index $CS(f_k)$ is defined as a statistical index at frequency f_k in Eq. (26).

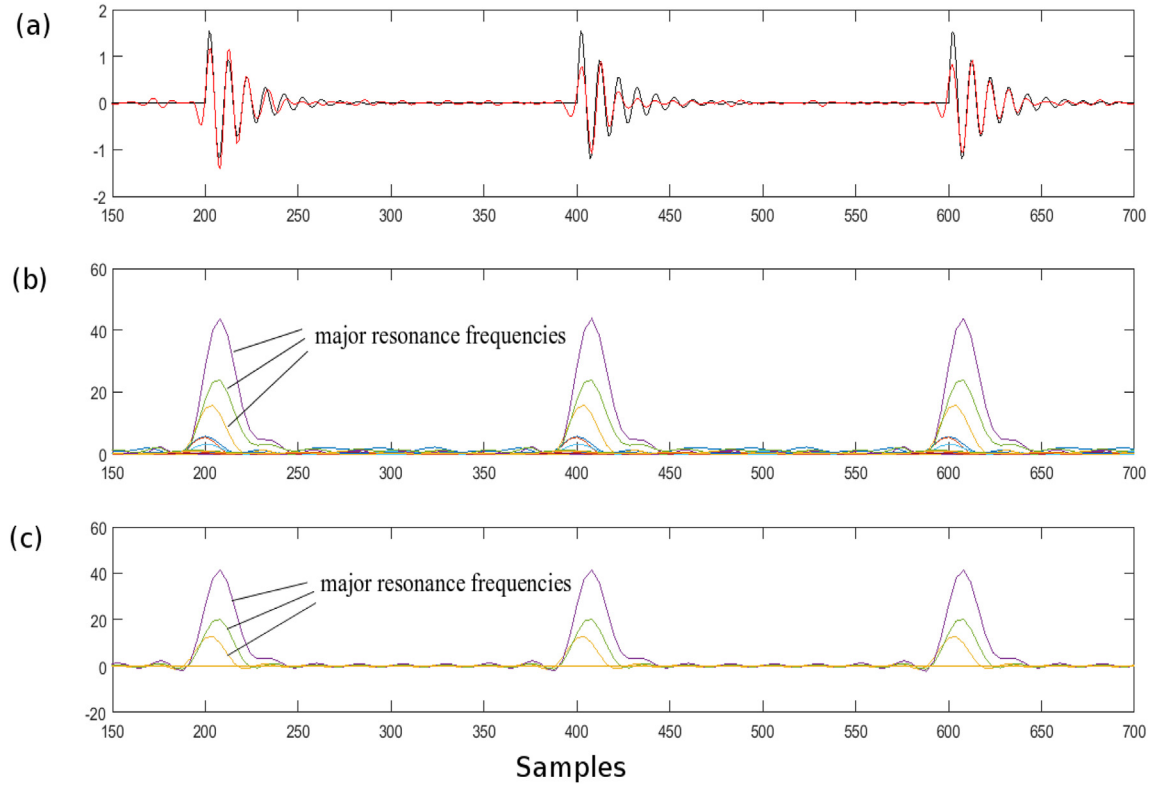

Fig. 9. (a) Enlarged view of the filtered time signal $\hat{x}[n]$ of Fig. 5 (b) and (c). (b) Initialized time-dependent variance of the CS signal, $\hat{\sigma}_x^2(i; f_k)^{[0]}$, and (c) the estimated $\hat{\sigma}_x^2(i; f_k)^{[k+1]}$ from the **EM** algorithm.

mechanical components are likely to produce periodic modulations of the vibration signals. Besides the transient signal, periodically-modulated signals (modulated white noise and modulated narrow-band noise) are also tested with as good performance as in Case 1.

In order to demonstrate the potential of the proposed scheme,

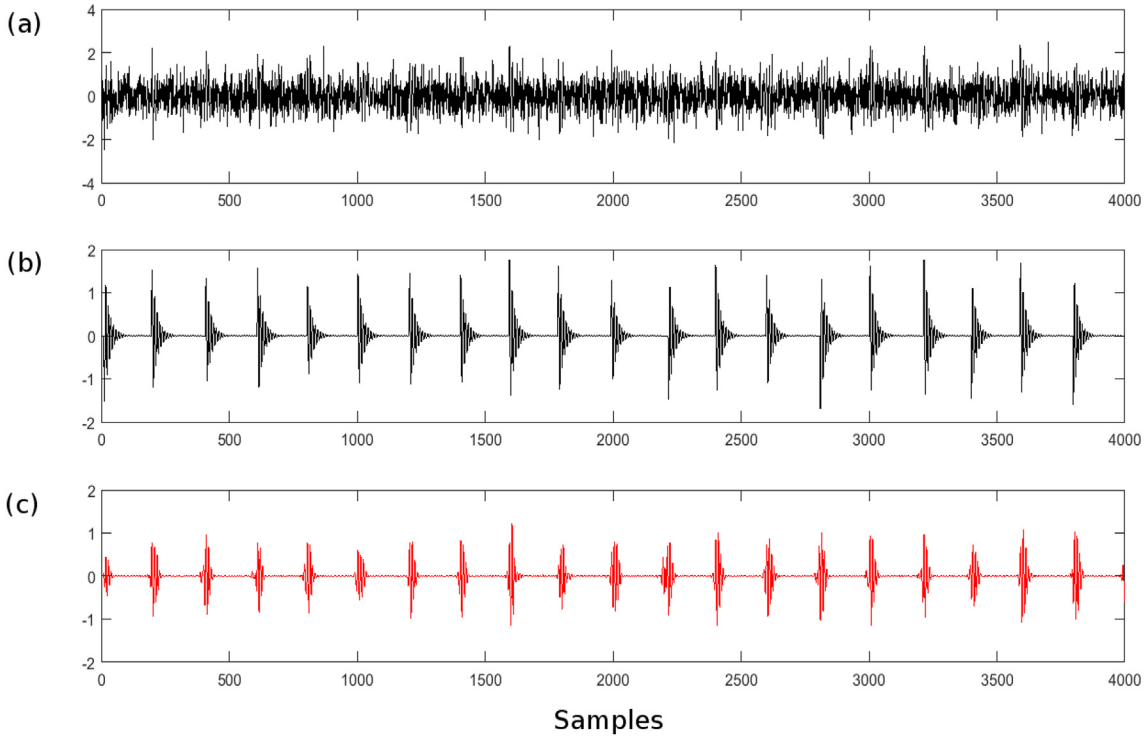

Fig. 10. (a) Synthetic signal of Case 2 with additive white noise (noise-to-signal-ratio = 6 dB. (b) Synthetic repetitive transient signal. (c) Filtered time signal $\widehat{x}[n]$.

Case 2 (repetitive transient signal) is generated by means of two random variables described as:

$$y(t) = \sum_{j=-\infty}^{+\infty} h(t - jT - \tau_j)A_j + n(t) \tag{38}$$

$$H(z) = \frac{b_1}{a_1 + a_2 \cdot z^{-1} + a_3 \cdot z^{-2}} \tag{39}$$

where $\tau_j \sim \mathcal{N}(\mu_\tau = 0, \sigma_\tau = 0.05T)$ and $A_j \sim \mathcal{N}(\mu_A = 0, \sigma_A = 0.1)$ account for the uncertainties on the arrival time and on the magnitude of the j^{th} transient, respectively. The white noise $n(t)$ is set with a noise-to-signal-ratio of 6 dB and the signal length is $L = 10^4$ samples. A second-order system is defined by Eq. (39), whose numerator and denominator coefficients are $\boldsymbol{b} = [1]$ and $\boldsymbol{a} = [1,\ -2cos(2\pi f_0)r,\ r^2]$ with $r = 0.95$, respectively.

Fig. 10 (a) and (b) show the signal and the synthetic repetitive transient signal in time. It is highlighted that although these transients are not exactly periodic because the rolling elements experience some random slips, its corresponding parameters $\widehat{\sigma}_x^2(i;\, f_k)^{[0]}$ and $\widehat{\sigma}_x^2(i;\, f_k)^{[k+1]}$ both provide good performances as displayed in Fig. 11 (a) and (b). In addition, the spectrogram of the estimated CS signal $\widehat{X}(i,\, f_k)$ still reveals distinct spectral contents with its periodic time-varying filter as seen in Fig. 11 (c) and (d), which are further verified by the recovered time signal $\widehat{x}[n]$ in Fig. 10 (c). It is seen from the enlarged view of $\widehat{x}[n]$ in Fig. 12 (a) that the transients are close to the reference, even though the frequency of these modulations are not integrally related to the mean transient repetition rate.[6] The corresponding parameters $\widehat{\sigma}_x^2(i;\, f_k)^{[0]}$ and $\widehat{\sigma}_x^2(i;\, f_k)^{[k+1]}$ are estimated as well as those of Case 1, but considerably wider as marked in Fig. 12 (b) and (c).

7. Examples of application

This section illustrates how the proposed method performs on real-world signals concerned with the diagnostics of rolling element bearings. Case 3 demonstrates its effectiveness on the database of the wind turbine gearboxes. In addition, the stochastic model addressing the issue of signal denoising and weak feature enhancement are can be easily extended to analyze poly-cyclostationary signals with different basic cycles. For instance, Case 4 evidences a marked signature of the rolling elements as well as a comparison of the results with the fast kurtogram; Case 5 achieves a multi-source separation – i.e., bearing and gear signals.

7.1. Case 3: CS signatures of wind turbine gearboxes

This first experiment deals with the dataset from a three-stage gearbox of the wind turbines in northern Sweden [43]. The vibration signals are related to the axial direction of an accelerometer mounted on the housing of the output shaft bearing as shown in Fig. 2. The sampling frequency is $f_k = 12.8$ kHz and each signal segment is 1.28s.

From inspection of Fig. 13, the required parameters of the STFT can be selected by following Eqs. (28)-(29), i.e. $N_w = 2^6$, $R = 8$. Fig. 14 (a) displays the spectrogram (magnitude of the STFT) of the raw signal with its periodic energy, which approximately dominates in the band $[1;\ 2]$ kHz. According to Eqs. (30)-(35), one can initialize the parameters of the **EM** algorithm. As a result, the recovered CS signal and time-dependent variance show a "cyclic behavior" at $1/T = 18.8$ Hz with evidence of spectral content in band $[1.4;\ 2]$ kHz, as seen in Fig. 14 (c) and (d), respectively. The CS

[6] Strictly speaking, such a signal is referred to as a quasi-cyclostationary, i.e. with an energy distribution that has no finite period but can still be expanded into a sum of Fourier series.

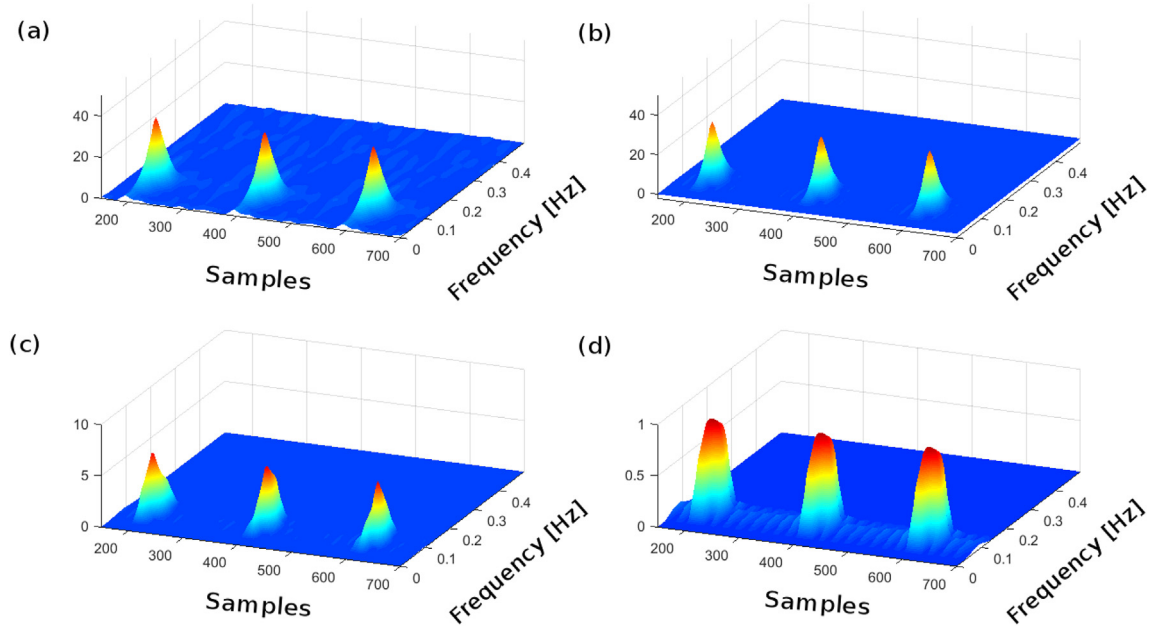

Fig. 11. (a) Initialized time-dependent variance of the CS signal, $\widehat{\sigma}_x^2(i;f_k)^{[0]}$, and (b) the estimated $\widehat{\sigma}_x^2(i;f_k)^{[k+1]}$ from the **EM** algorithm. (c) Spectrogram of the estimated CS signal, $\widehat{X}(i,f_k)$, with (d) its periodic time-varying filter $1/(1+H(i;f_k))$ as defined in Eqs. (14)-(15).

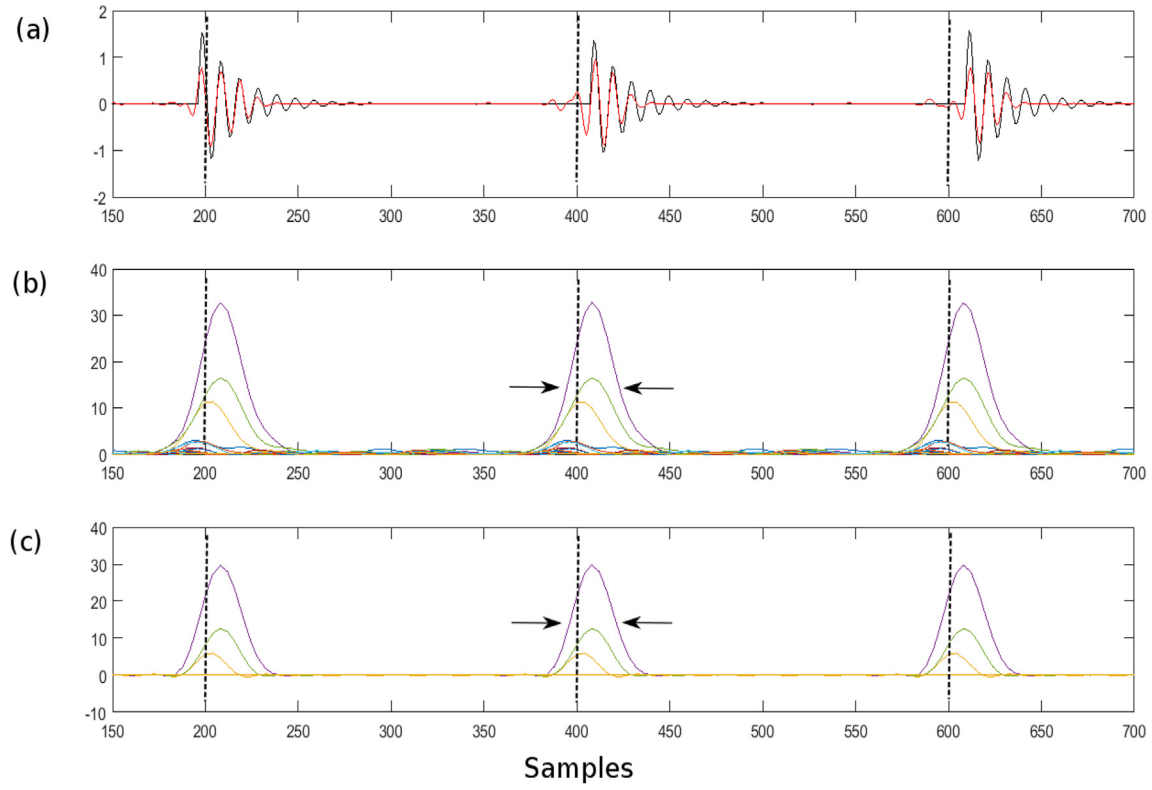

Fig. 12. (a) Enlarged view of the filtered time signal $\widehat{x}[n]$ of Fig. 10 (b) and (c). (b) Initialized time-dependent variance of the CS signal, $\widehat{\sigma}_x^2(i;f_k)^{[0]}$, and (c) the estimated $\widehat{\sigma}_x^2(i;f_k)^{[k+1]}$ from the **EM** algorithm.

index $CS(f_k)$ is further calculated to quantify the strength of SOI over the carrier frequency f_k as illustrated in Fig. 15. In particular, the accelerometric sensor (which is close to output shaft bearing) clearly evidences the dominant harmonics of the shaft rotation with the carrier frequency band $[1.4;\ 2]$ kHz, which probably corresponds to the misalignment of the bearing, mechanical looseness, etc. Since the CS index provides an indication of the fault severity, it is highly recommended to perform maintenance actions, even though no typical signature of bearing failures is displayed. Concerning the dataset, it proves the evidence of the periodic

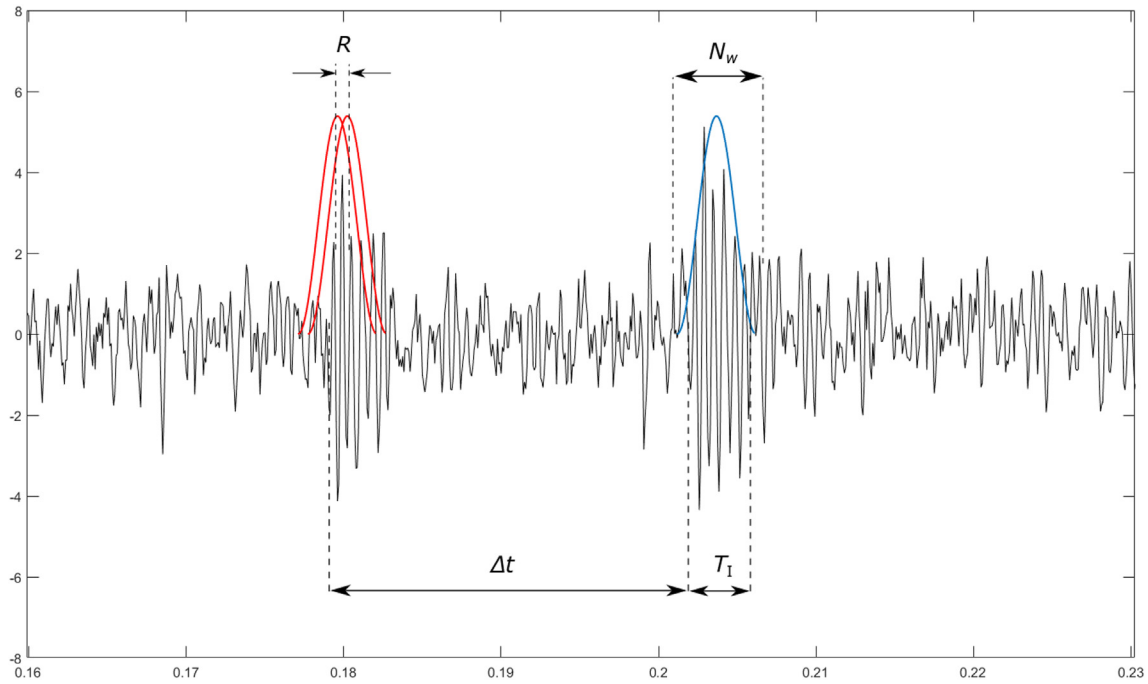

Fig. 13. Selection of the window length N_w and shift R with respect to transient durations T_I and cycle Δt.

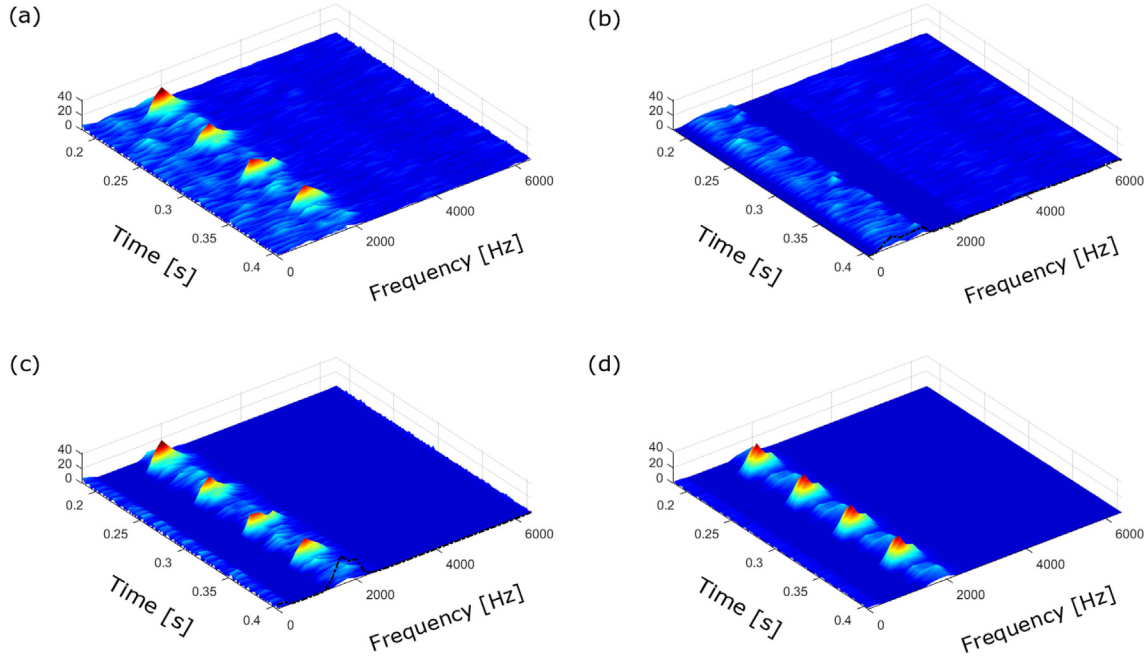

Fig. 14. Spectrogram (magnitude of the STFT) of (a) the raw signal $|Y(i, f_k)|$, (b) the noise signal $|R(i, f_k)|$ and (c) the recovered CS signal $|X(i, f_k)|$ (Note: the classical power spectrum can be approximated by taking the time-average of the spectrogram as marked in black dash-dot lines.). (d) The extracted feature by means of the time-dependent variance $\sigma_x^2(i; f_k)^{|k+1|}$.

energy flow in wind turbine gearboxes, yet lacking the sophisticated examples submerged by interfering sources. Case 4 and 5 are therefore analyzed to further validate the effectiveness of the proposed method.

7.2. Case 4: an incipient ball fault

In the following, two typical types of bearing fault (i.e. inner race and ball fault) are investigated in a dataset from the Vibrations and Acoustics Laboratory of the University of New South Wales (Sydney) [44]. The test-rig is a one-stage gearbox with primary and secondary shafts supported by ball bearings.

The parameter settings are reported in Table 1 for the tested signals in Case 4 and Case 5, respectively.

The first test deals with an incipient bearing damage on the rolling elements (i.e. ball fault), yet in the presence of strong gear

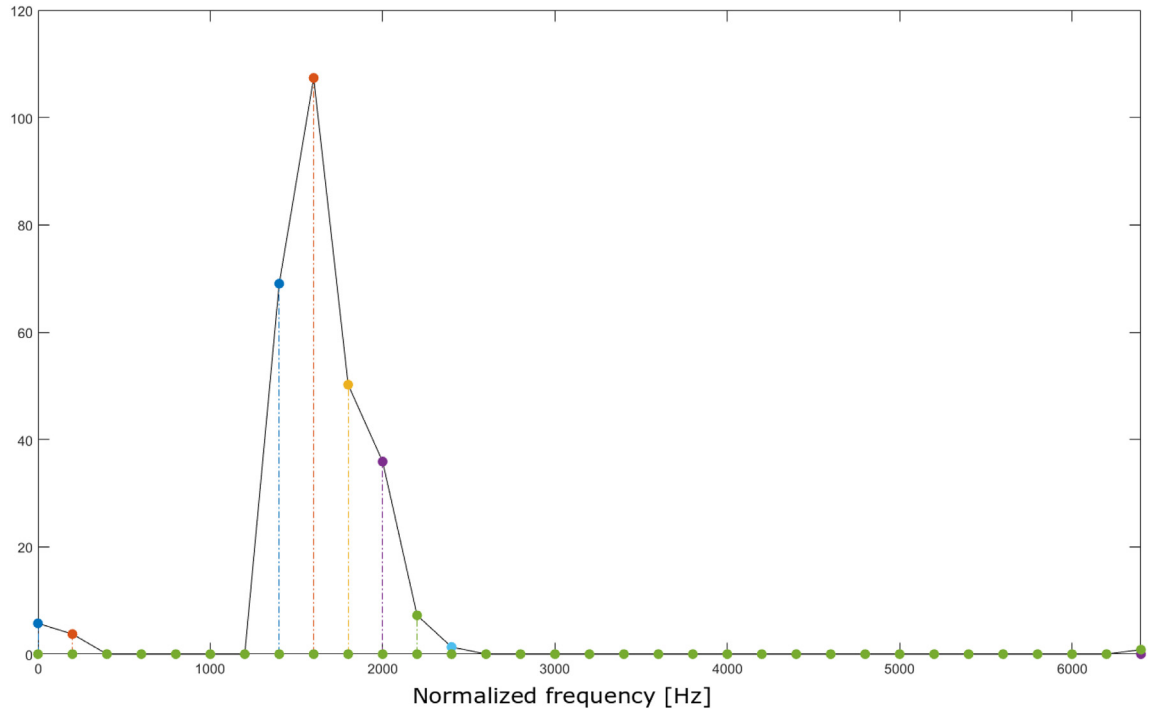

Fig. 15. Cyclostationary index $CS(f_k)$ is defined as a statistical index at frequency f_k in Eq. (26).

Table 1
Parameter settings used in Case 4 and Case 5.

	Case 4	Case 5
Sampling frequency F_s (kHz)	48	
Duration (s)	1.365	2.082
N_w	2^6	2^7
R	8	16
Rotation frequency – f_{rot} (Hz)	10	6
Gear mesh frequency – f_g (Hz)	320	192
Cage frequency – FTF (Hz)	4.1	
Ball spin frequency – BSF (Hz)	26.1	
Ball pass frequency on inner race – BPFI (Hz)		42.8

vibrations, thus under a relatively low signal-to-noise ratio (SNR).

Fig. 16 shows the spectrogram (logarithmic scale) of the raw signal in conjunction with marked periodic energy flow ($1/T = 2\times BSF$, dashed line in red). Moreover, Fig. 17 (a) illustrates the waveform of the measured signal, from which no obvious impulses can be observed. By means of the proposed method, the signal is therefore divided into the filtered part $x[n]$ (driven by $1/T = 2\times BSF$ Hz) and the noise (residual) part $r[n]$, as presented in Fig. 17 (c) and (d) respectively.

It is seen from Fig. 18 (a) that there exists non-stationary components in the high frequency band above 10 kHz, whereas the low frequency range is dominated by high energy components related to the gearbox vibrations. In particular, the former component evidences a "cyclic behavior" at $1/T = 2\times BSF$ Hz, as also seen in Fig. 18 (b) and (c). Additionally, Fig. 18 (d) clearly reveals the time-dependent variance in the time-frequency plane.

Since the information of the bearing fault is completely masked by high-energy components from the gearbox, the fast kurtogram is therefore applied as a comparison to demonstrate the capability of the proposed method. As seen in Fig. 19, there exists several local maxima in the kurtogram, one maximum is therefore taken at 73.2 whose corresponding to the frequency band [13.5; 15] kHz. Fig. 17 (b) displays the band-pass filtered signal in band [13.5; 15] kHz, which clearly evidences the transient nature similar to the filtered part $x[n]$ in Fig. 17 (c).

On closer inspection, Fig. 20 highlights that the signal is composed of a series of repetitive transients hidden under gear vibrations. In particular, Fig. 20 (b) and (c) compare the enlarged view of results based on the kurtogram and the proposed time-dependent filter. As compared to the classical methodology, the proposed one achieves an exact location of the transients with their full-band spectral content. This may be used advantageously to better characterize the fault signature, infer the fault dimension and spectral content, and possibly update trend models for prognostics.

Furthermore, due to the high-energy interferences, the conventional envelope analysis (SES) fails to detect the fault signatures, whereas the filtered time signal confirms the existence of bearing ball fault (see Fig. 21). Comparing with Fig. 21 (b), the spectrum of Fig. 21 (c) better enhances the odd harmonics of the BSF than the SES from the kurtogram, even if the diagnostics information is very similar in both cases.

7.3. Case 5: separation of bearing and gear signatures

This last case resembles very much the previous one, yet with only the signature of the inner race. Note that the energy of the gear vibrations is found significantly higher than that of bearing BPFI. Moreover, due to the close physical connection of the gear and bearing elements, the acquired signal shows a mixture of the two types of signal over the whole frequency range – see Fig. 22 (a). Here again, both the bearing and gear signatures are distinctly extracted as the SOI, as shown in Fig. 22 (b) and (c), respectively. It is further verified in Fig. 22 (d) that there exists a crossing point around 6 kHz.

Fig. 23 (a) and (b) display the CS indices $CS(f_k)$, which respectively indicate the strength of source 1 and 2 over the carrier frequency f_k, related to the bearing and gear signature.

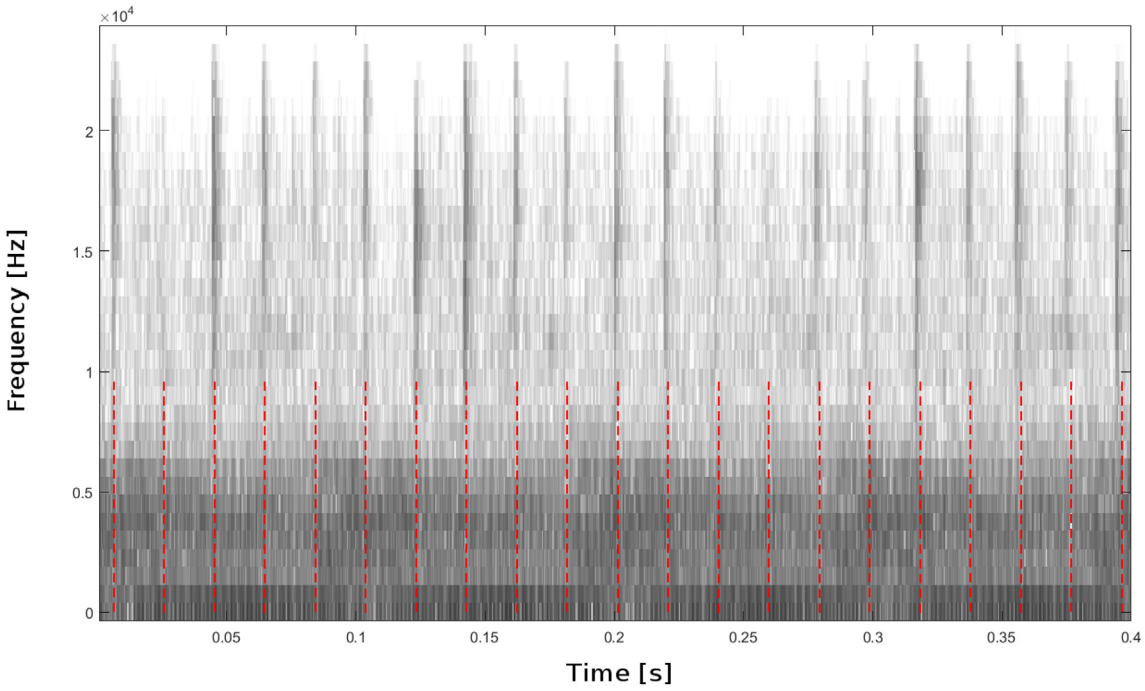

Fig. 16. Spectrogram (logarithmic scale) of the signal in Case 4 (frequency resolution $\Delta f = 750$ Hz) with evidence of spectral content in band [9.75; 23.25] kHz.

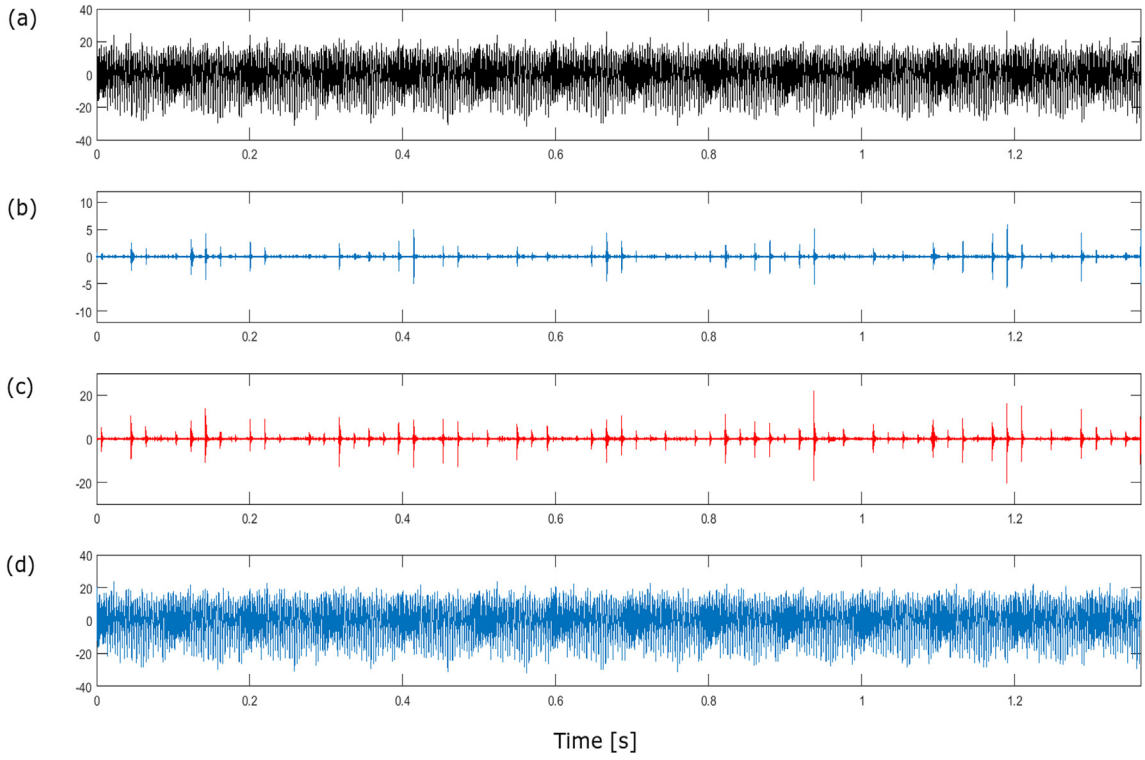

Fig. 17. Case 4. Vibration waveform of (a) the raw signal, (b) the band-pass filtered signal in the frequency band [13.5; 15] kHz returned by the fast kurtogram, (c) the filtered time signal $x[n]$ driven by $1/T = 2 \times BSF$ Hz from the proposed full-band time-dependent filter and (d) the noise (residual) signal $r[n]$.

Fig. 24 shows a zoomed view of the vibration waveform, divided into the filtered parts of source 1 and 2. The detection of the fault is further demonstrated by means of the SES computed in these components in Fig. 25. The periodic-variance based model clearly evidences the dominant harmonics of the gear mesh frequency with sidebands at the shaft rotation, contrary to the classical SES of the raw signal which has a poorer SNR.

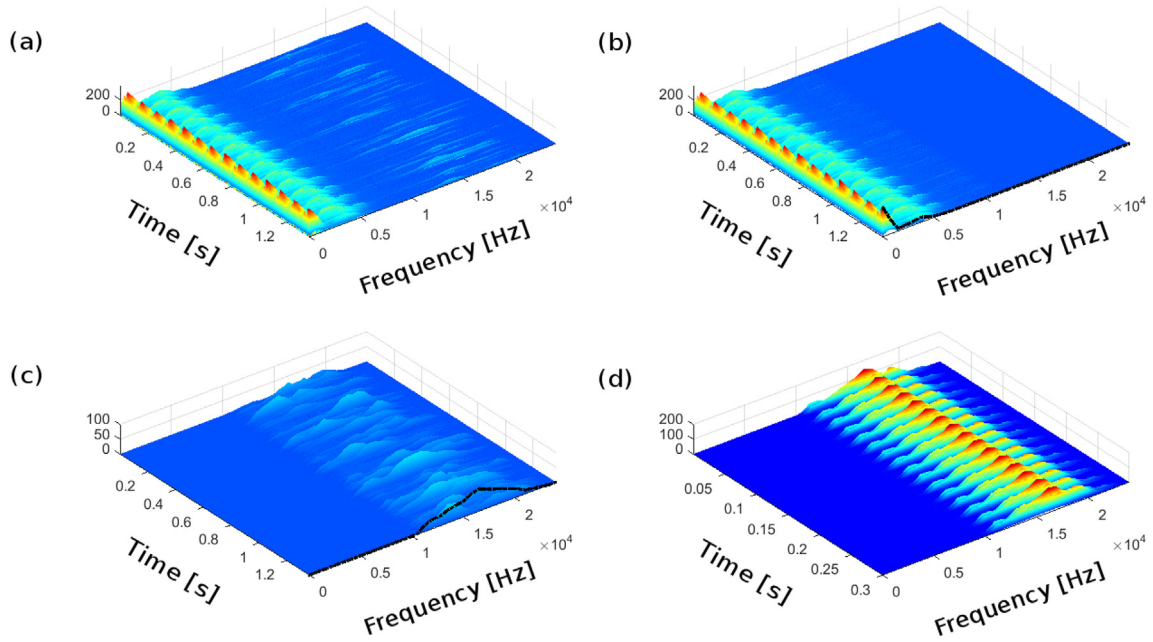

Fig. 18. Spectrogram (magnitude of the STFT) of (a) the raw signal $|Y(i, f_k)|$, (b) the noise signal $|R(i, f_k)|$ and (c) the recovered CS signal $|X(i, f_k)|$ with evidence of spectral content in band [9.75; 23.25] kHz (Note: the classical power spectrum can be approximated by taking the time-average of the spectrogram as marked in black dash-dot lines.). (d) The extracted feature by means of the time-dependent variance $\sigma_x^2(i; f_k)^{[k+1]}$.

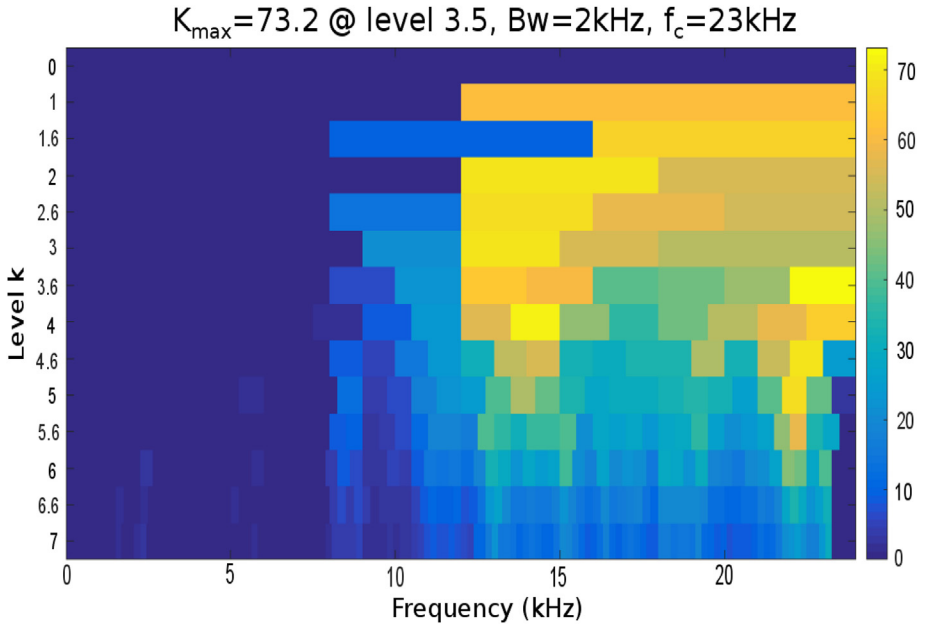

Fig. 19. Kurtogram of signal of Case 4 computed over $K = 7$ levels with a 1/3-binary tree and an 8 coefficient prototype filter. Several local maxima are presented. One relevant maximum is taken to the frequency band [13.5; 15] kHz.

8. Conclusions

This paper has introduced a new stochastic model, namely periodic-variance based model, to extract a signal of interest (SOI) masked by other interfering signals – a typical situation where classical vibrodiagnostic method are prone to fail. The SOI is supposed CS signals recorded at constant regime with an individual "periodicity" that is different from the other sources. This allows a semi-blind full-band extraction of the SOI through application of self-tailored time-dependent filter, which may be seen as an extension of the Wiener filter. Although it requires the knowledge of the cyclic frequency of the SOI, it is noteworthy that it is semi-blind in the sense that nothing else is assumed (e.g. the number of interferences, their statistics and the noise properties); besides, the cyclic frequency may be known from the machine kinematics or alternatively can be estimated from the observed signals. Moreover, it applies to most common types of modulations in mechanical systems as a result of an open module that can be tailored accordingly by the user.

Unlike other analytical approaches, the proposed method is

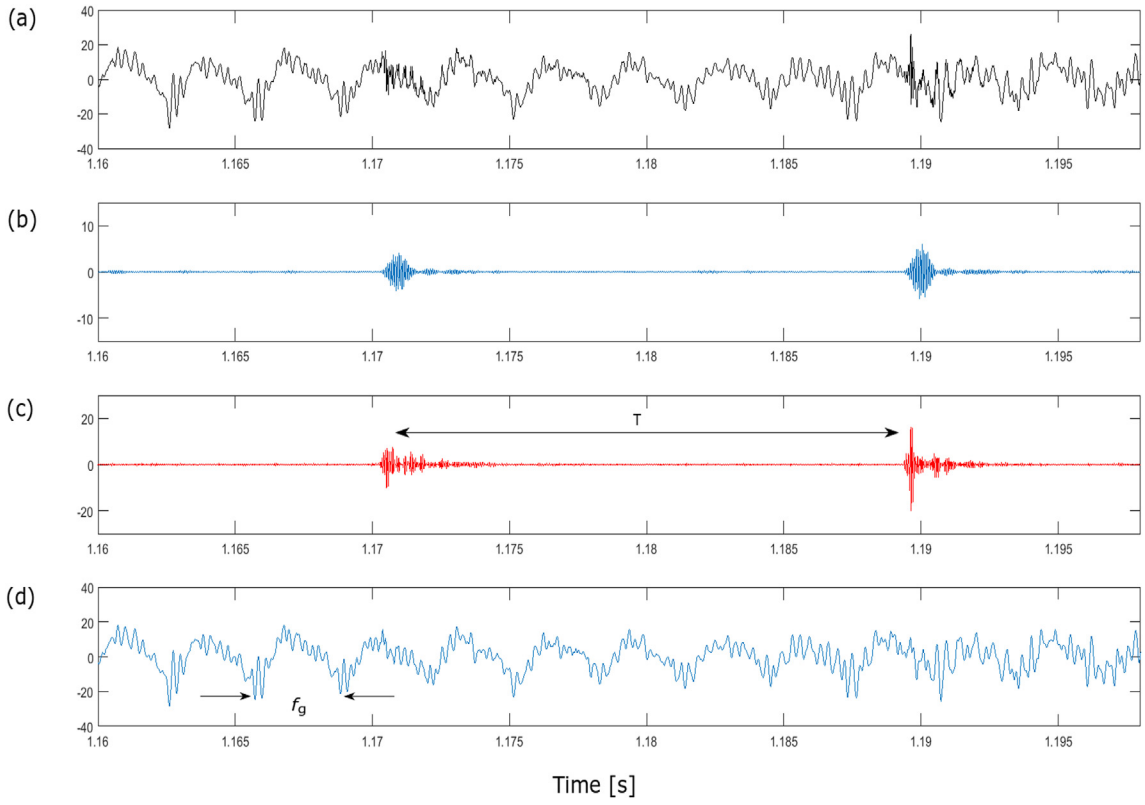

Fig. 20. Case 4. Enlarged view of (a) the vibration waveform $y[n]$, (b) the band-pass filtered signal in the frequency band [13.5; 15] kHz, (c) the filtered time signal $x[n]$ driven by $1/T = 2 \times BSF$ Hz and (d) the noise (residual) signal $r[n]$.

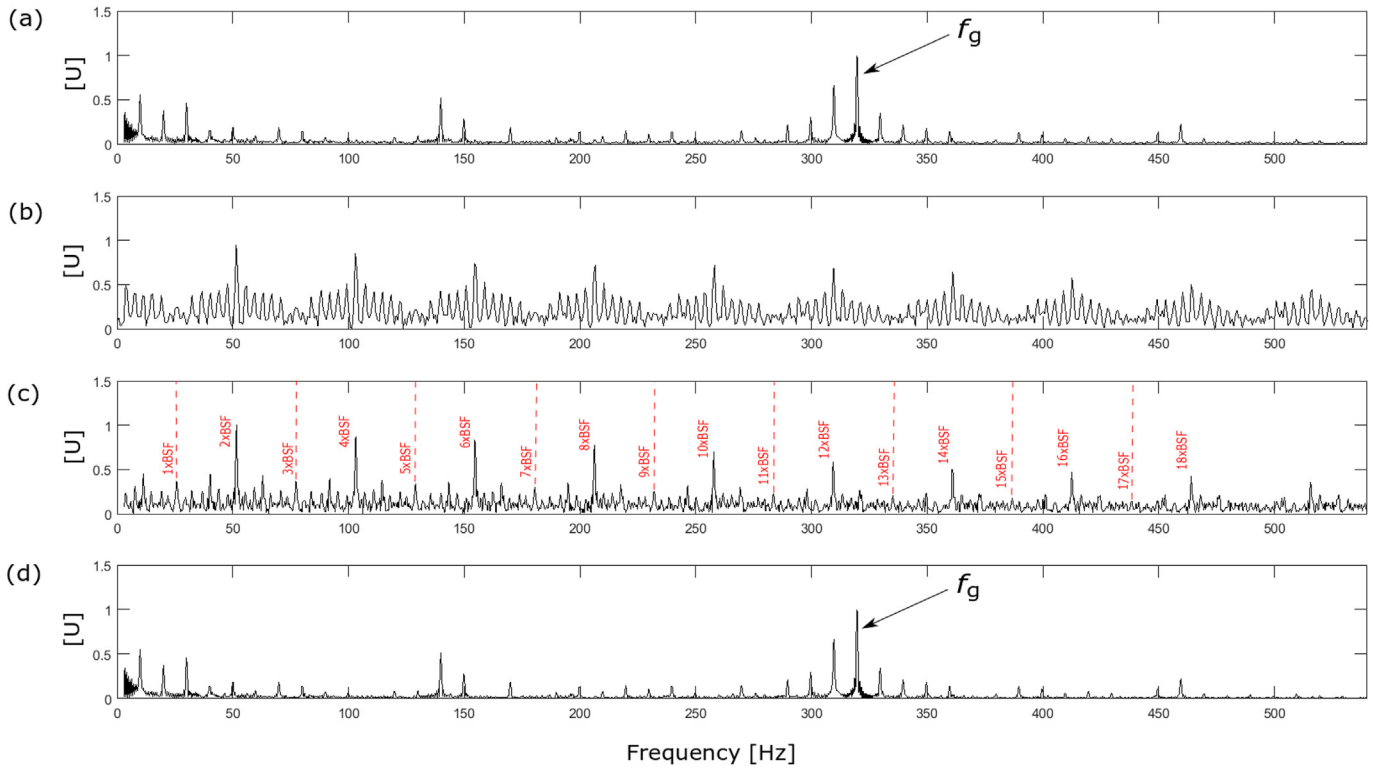

Fig. 21. Case 4. Squared Envelope Spectrum of (a) the vibration waveform: $S_y^{SES}(\alpha)$, (b) the band-pass filtered signal returned by the fast kurtogram, (c) the filtered time signal: $S_x^{SES}(\alpha)$ and (d) the noise (residual) signal: $S_r^{SES}(\alpha)$.

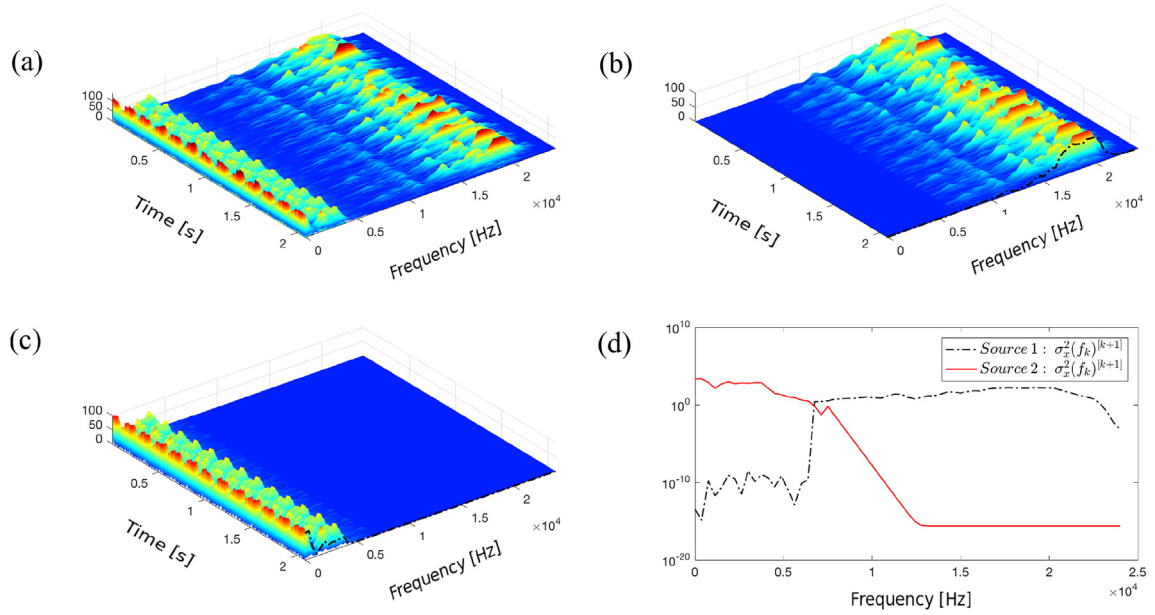

Fig. 22. Spectrogram (magnitude of the STFT) of (a) the raw signal $|Y(i, f_k)|$, (b) the first cyclic source $\left|X^1(i, f_k)\right|$ and (c) the second cyclic source $\left|X^2(i, f_k)\right|$ (the classical power spectrum is approximated by taking the time-average of the spectrogram as marked in black dash-dot lines.). (d) The extracted feature by taking the mean value of $\sigma_x^2(i; f_k)^{[k+1]}$ over the time instants i.

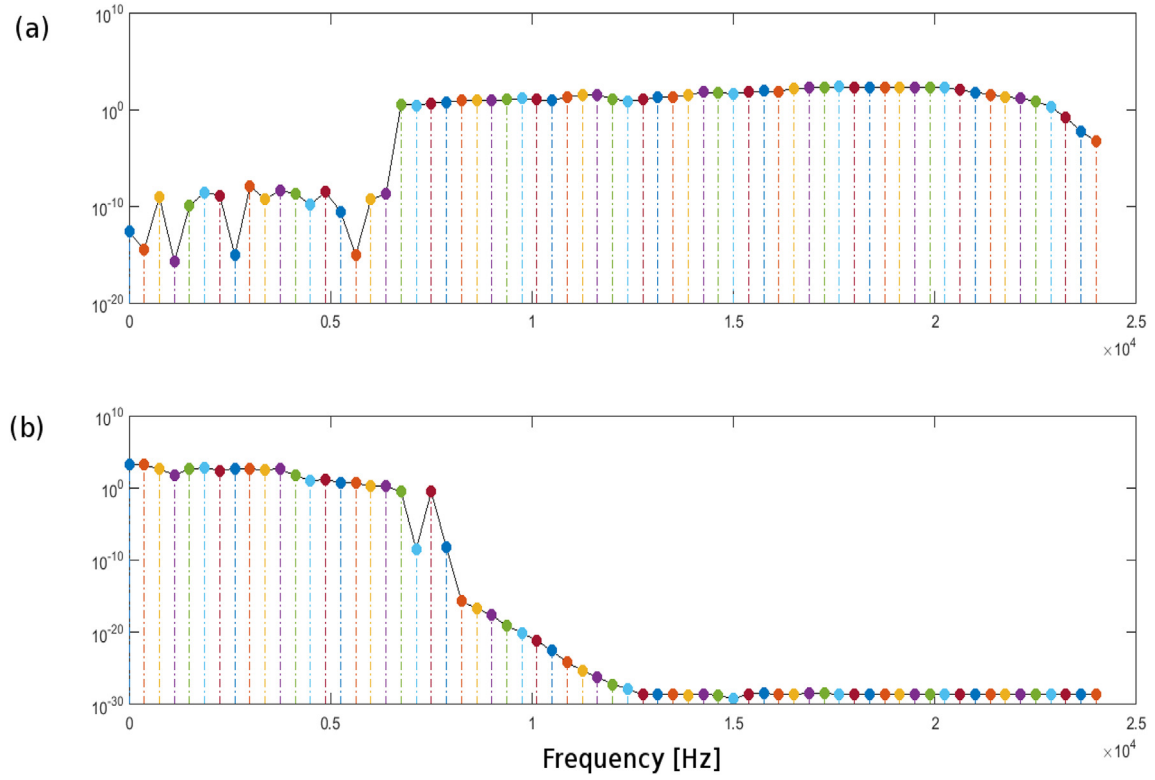

Fig. 23. Cyclostationary index $CS(f_k)$ of (a) source 1 and (b) source 2, defined in Eq. (26).

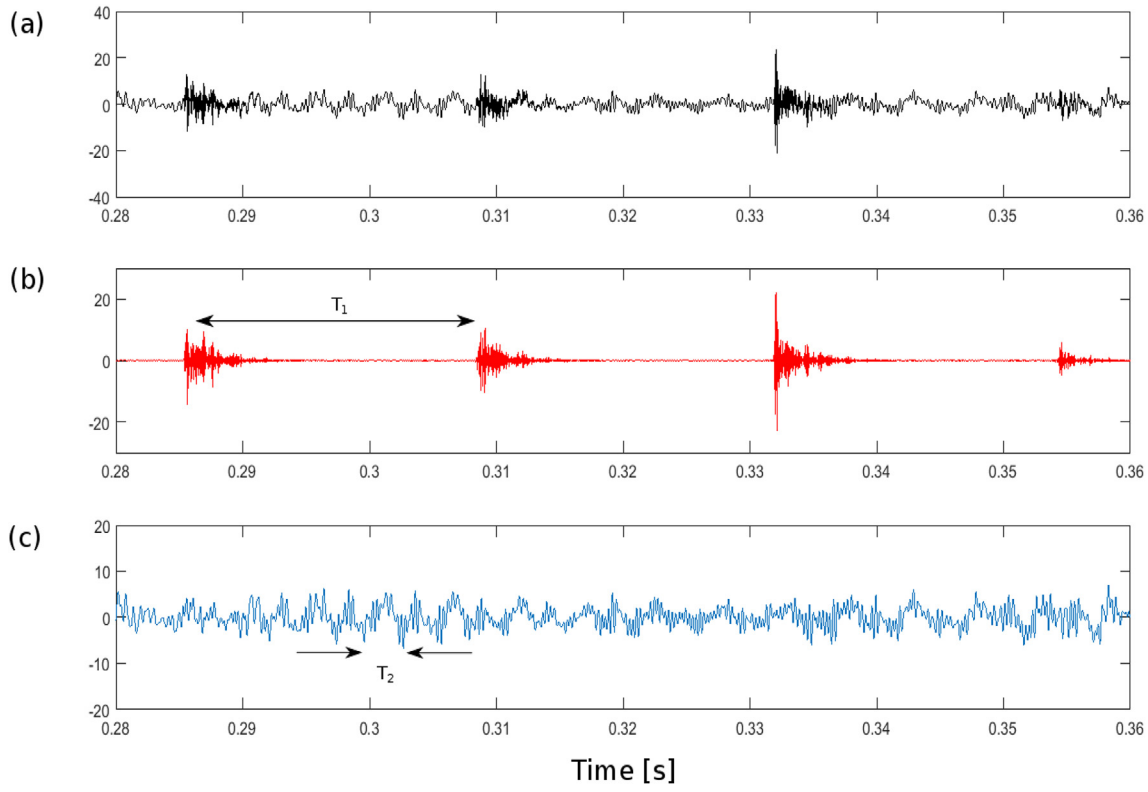

Fig. 24. Case 5. Enlarged view of (a) the vibration waveform $y[n]$, (b) the filtered time signal of source 1: $x^1[n]$ driven by $1/T_1 = BPFI$ Hz and (c) that of source 2: $x^2[n]$ driven by $1/T_2 = f_g = f_{rot} \times$ No. of teeth Hz.

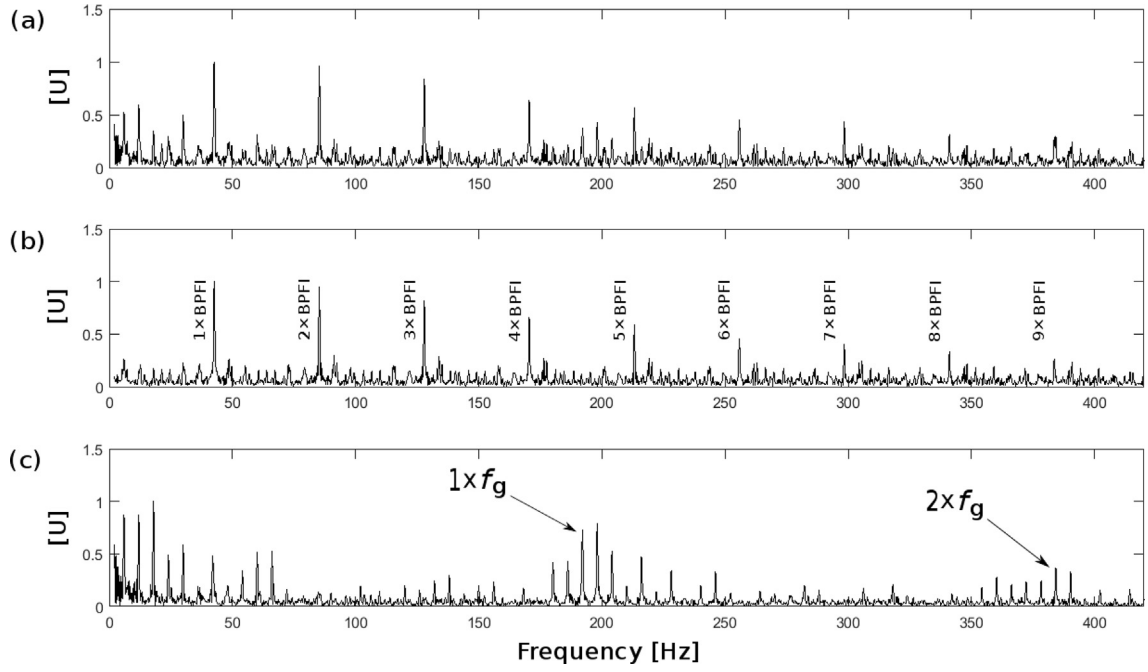

Fig. 25. Case 5. Squared Envelope Spectrum of (a) the vibration waveform: $S_y^{SES}(\alpha)$, (b) the filtered time signal of source 1: $S_{x^1}^{SES}(\alpha)$ and (c) that of source 2: $S_{x^2}^{SES}(\alpha)$.

tailored to the data which leads to high adaptability and flexibility. The performance is however based on the time CS assumption (instead of the angle CS assumption) and is thus limited to analyze machine signals captured under invariant operating conditions. Its advantage resides in providing a *perfect* extraction of the SOI in the noiseless case. Eventually, this paper has illustrated how it can be extened to extract two sources – i.e. bearings and gears – which is quite common in gearboxes of wind turbine.

Acknowledgments

This work was supported financially by the National Natural Science Foundation of China (Grant No. 51905029), the Fundamental Research Funds for the Central University (Grant No. 2018RC009), a scholarship from the China Scholarship Council (Grant No. 201304490040) and was performed within the framework of the Labex CeLyA of University of Lyon, operated by the French National Research Agency.

References

[1] J. Antoni, Blind separation of vibration components: principles and demonstrations, Mech. Syst. Signal Process. 19 (6) (2005) 1166–1180.
[2] Z. Feng, S. Qin, M. Liang, Time–frequency analysis based on vold-kalman filter and higher order energy separation for fault diagnosis of wind turbine planetary gearbox under nonstationary conditions, Renew. Energy 85 (2016) 45–56.
[3] F.P.G. Márquez, A.M. Tobias, J.M.P. Pérez, M. Papaelias, Condition monitoring of wind turbines: techniques and methods, Renew. Energy 46 (2012) 169–178.
[4] H.D.M. de Azevedo, A.M. Araújo, N. Bouchonneau, A review of wind turbine bearing condition monitoring: state of the art and challenges, Renew. Sustain. Energy Rev. 56 (2016) 368–379.
[5] Y. Lei, J. Lin, M.J. Zuo, Z. He, Condition monitoring and fault diagnosis of planetary gearboxes: a review, Measurement 48 (2014) 292–305.
[6] W. Liu, B. Tang, J. Han, X. Lu, N. Hu, Z. He, The structure healthy condition monitoring and fault diagnosis methods in wind turbines: a review, Renew. Sustain. Energy Rev. 44 (2015) 466–472.
[7] W. Liu, A review on wind turbine noise mechanism and de-noising techniques, Renew. Energy 108 (2017) 311–320.
[8] T. Wang, Q. Han, F. Chu, Z. Feng, Vibration based condition monitoring and fault diagnosis of wind turbine planetary gearbox: a review, Mech. Syst. Signal Process. 126 (2019) 662–685.
[9] A. Romero, S. Soua, T.-H. Gan, B. Wang, Condition monitoring of a wind turbine drive train based on its power dependant vibrations, Renew. Energy 123 (2018) 817–827.
[10] W. Teng, X. Ding, Y. Zhang, Y. Liu, Z. Ma, A. Kusiak, Application of cyclic coherence function to bearing fault detection in a wind turbine generator under electromagnetic vibration, Mech. Syst. Signal Process. 87 (2017) 279–293.
[11] P. McFadden, J. Smith, Vibration monitoring of rolling element bearings by the high-frequency resonance technique–a review, Tribol. Int. 17 (1) (1984) 3–10.
[12] J. Antoni, Cyclic spectral analysis of rolling-element bearing signals: facts and fictions, J. Sound Vib. 304 (3 - 5) (2007) 497–529.
[13] D. Abboud, J. Antoni, S. Sieg-Zieba, M. Eltabach, Envelope analysis of rotating machine vibrations in variable speed conditions: a comprehensive treatment, Mech. Syst. Signal Process. 84 (2017) 200–226.
[14] A. Ming, W. Zhang, Z. Qin, F. Chu, Envelope calculation of the multi-component signal and its application to the deterministic component cancellation in bearing fault diagnosis, Mech. Syst. Signal Process. 50 (2015) 70–100.
[15] J. Antoni, The spectral kurtosis: a useful tool for characterising non-stationary signals, Mech. Syst. Signal Process. 20 (2) (2006) 282–307.
[16] J. Antoni, R. Randall, The spectral kurtosis: application to the vibratory surveillance and diagnostics of rotating machines, Mech. Syst. Signal Process. 20 (2) (2006) 308–331.
[17] J. Antoni, The infogram: entropic evidence of the signature of repetitive transients, Mech. Syst. Signal Process. 74 (2016) 73–94.
[18] D. Wang, An extension of the infograms to novel bayesian inference for bearing fault feature identification, Mech. Syst. Signal Process. 80 (2016) 19–30.
[19] C. Li, D. Cabrera, J.V. de Oliveira, R.-V. Sanchez, M. Cerrada, G. Zurita, Extracting repetitive transients for rotating machinery diagnosis using multiscale clustered grey infogram, Mech. Syst. Signal Process. 76 (2016) 157–173.
[20] H. Qiu, J. Lee, J. Lin, G. Yu, Wavelet filter-based weak signature detection method and its application on rolling element bearing prognostics, J. Sound Vib. 289 (4) (2006) 1066–1090.
[21] W. Teng, X. Ding, X. Zhang, Y. Liu, Z. Ma, Multi-fault detection and failure analysis of wind turbine gearbox using complex wavelet transform, Renew. Energy 93 (2016) 591–598.
[22] W. Teng, X. Ding, H. Cheng, C. Han, Y. Liu, H. Mu, Compound faults diagnosis and analysis for a wind turbine gearbox via a novel vibration model and empirical wavelet transform, Renew. Energy 136 (2019) 393–402.
[23] J. Wang, Q. He, F. Kong, Multiscale envelope manifold for enhanced fault diagnosis of rotating machines, Mech. Syst. Signal Process. 52 (2015) 376–392.
[24] A. Ming, W. Zhang, Z. Qin, F. Chu, Fault feature extraction and enhancement of rolling element bearing in varying speed condition, Mech. Syst. Signal Process. 76 (2016) 367–379.
[25] G. Xin, N. Hamzaoui, J. Antoni, Semi-automated diagnosis of bearing faults based on a hidden markov model of the vibration signals, Measurement 127 (2018) 141–166.
[26] G. Xin, Y. Qin, L.-M. Jia, S.-J. Zhang, J. Antoni, Low-rank and sparse model: a new perspective for rolling element bearing diagnosis, in: 2018 International Conference on Intelligent Rail Transportation (ICIRT), IEEE, 2018, pp. 1–5.
[27] J. Antoni, Cyclostationarity by examples, Mech. Syst. Signal Process. 23 (4) (2009) 987–1036.
[28] J. Antoni, G. Xin, N. Hamzaoui, Fast computation of the spectral correlation, Mech. Syst. Signal Process. 92 (2017) 248–277.
[29] I. Antoniadis, G. Glossiotis, Cyclostationary analysis of rolling-element bearing vibration signals, J. Sound Vib. 248 (5) (2001) 829–845.
[30] C. Capdessus, M. Sidahmed, J. Lacoume, Cyclostationary processes: application in gear faults early diagnosis, Mech. Syst. Signal Process. 14 (3) (2000) 371–385.
[31] J. Antoni, F. Bonnardot, A. Raad, M.E. Badaoui, Cyclostationary modelling of rotating machine vibration signals, Mech. Syst. Signal Process. 18 (6) (2004) 1285–1314.
[32] J. Antoni, Cyclic spectral analysis in practice, Mech. Syst. Signal Process. 21 (2) (2007) 597–630.
[33] F. Bonnardot, R. Randall, F. Guillet, Extraction of second-order cyclostationary sources–application to vibration analysis, Mech. Syst. Signal Process. 19 (6) (2005) 1230–1244.
[34] R. Boustany, J. Antoni, A subspace method for the blind extraction of a cyclostationary source: application to rolling element bearing diagnostics, Mech. Syst. Signal Process. 19 (6) (2005) 1245–1259.
[35] Y. Ming, J. Chen, G. Dong, Weak fault feature extraction of rolling bearing based on cyclic wiener filter and envelope spectrum, Mech. Syst. Signal Process. 25 (5) (2011) 1773–1785.
[36] J. Urbanek, T. Barszcz, R. Zimroz, J. Antoni, Application of averaged instantaneous power spectrum for diagnostics of machinery operating under non-stationary operational conditions, Measurement 45 (7) (2012) 1782–1791.
[37] J. Urbanek, T. Barszcz, J. Antoni, Time–frequency approach to extraction of selected second-order cyclostationary vibration components for varying operational conditions, Measurement 46 (4) (2013) 1454–1463.
[38] P. Kruczek, J. Obuchowski, A. Wylomanska, R. Zimroz, Cyclic sources extraction from complex multiple-component vibration signal via periodically time varying filter, Appl. Acoust. 126 (2017) 170–181.
[39] D.R. Brillinger, Time Series: Data Analysis and Theory, SIAM, 2001.
[40] G. Xin, Sparse Representations in Vibration-Based Rolling Element Bearing Diagnostics, Ph.D. thesis, University of Lyon, 2017.
[41] D.G. Luenberger, Y. Ye, Linear and Nonlinear Programming, Addison-wesley, Reading, MA, 1984.
[42] A. Logothetis, V. Krishnamurthy, Expectation maximization algorithms for map estimation of jump markov linear systems, IEEE Trans. Signal Process. 47 (8) (1999) 2139–2156.
[43] D.S.S. Martin del Campo Barraza, F. Sandin, Dataset Concerning the Vibration Signals from Wind Turbines in Northern sweden, 2018 available online, http://ltu.diva-portal.org/smash/record.jsf?pid=diva2.
[44] J. Antoni, Fast computation of the kurtogram for the detection of transient faults, Mech. Syst. Signal Process. 21 (1) (2007) 108–124.